Multiphoton excitation, ionization, and dissociation decay dynamics of small clusters of niobium, tantalum, and tungsten: Timeresolved thermionic emission

Andreas Amrein, Richard Simpson, and Peter Hackett

Citation: The Journal of Chemical Physics **95**, 1781 (1991); doi: 10.1063/1.461026
View online: http://dx.doi.org/10.1063/1.461026
View Table of Contents: http://scitation.aip.org/content/aip/journal/jcp/95/3?ver=pdfcov
Published by the AIP Publishing

Multiphoton excitation, ionization, and dissociation decay dynamics of small clusters of niobium, tantalum, and tungsten: Time-resolved thermionic emission

Andreas Amrein, Richard Simpson, and Peter Hackett
Steacie Institute for Molecular Sciences, National Research Council, 100 Sussex Drive, Ottawa, Ontario, Canada, K1A0R6

(Received 8 February 1991; accepted 26 April 1991)

The ionization dynamics of transition metal clusters have been investigated using time-of-flight mass and electron spectroscopy following single-photon (220 nm) and two-photon (351, 308, and 248 nm) excitation by pulsed laser light. At 220 nm, the ionization is direct and only prompt photoelectrons are produced. At 308 nm, delayed photoelectrons are produced. In consequence of this delayed ionization process, the time-of-flight mass spectrum peaks show exponential tails (decay time 0.67, 0.40, and 1.54 μs for Nb_7^+, Ta_7^+, and W_7^+, respectively). The decay time is shown to have an explicit dependence upon the cluster nuclearity and the laser wavelength. Experiments, in which the acceleration voltage of the time-of-flight spectrometer is pulsed on after the photoionization laser pulse, reveal that the precursor to the delayed ion signals is a neutral molecule, further evidence for a delayed ionization process. Similar effects are also seen for transition metal carbide clusters. Clusters of the same nuclearity have approximately equal decay times independent of the number of carbon atoms in the cluster. Transition metal oxide clusters do not give a two-photon ionization signal. These observations are explained using a model for the two-photon excitation, dissociation, and ionization dynamics. The central feature of this model is that following single photon excitation of an electronic transition below the ionization potential, there is rapid internal conversion among all vibronic states. The absorption of a second photon then creates a vibrationally excited cluster which contains internal energy greater than the ionization potential, but which can only ionize by a nonadiabatic process. This delayed ionization process occurs in competition with dissociation. As clusters of niobium, tantalum, and tungsten and their carbides are very strongly bound, the dissociation rate is slow and the delayed ionization may be observed. Oxidized clusters are expected to be less strongly bound as the diatomic transition metal oxide provides an excellent leaving group; in consequence, no delayed ionization is observed for partially oxidized clusters. The rates for dissociation and ionization of the bare metal clusters have been calculated within the framework of a generalized statistical theory for cluster processes. These rates are in general agreement with the measured decay times. In addition, the rates have been estimated by a procedure which uses tabulated thermodynamic parameters for the bulk elemental materials and makes an explicit correction for the size dependence. Once again, a reasonable agreement is obtained. These results provide the first experimental observation of a delayed ionization process for a neutral polyatomic molecular system. In analogy with materials properties, they also represent the first experimental observation of time-resolved thermionic emission.

I. INTRODUCTION

Small metal clusters offer the possibility of finite models for the extended metallic state. It has often been held that the study of such species will lead to a better understanding of the properties of materials.[1-26] An important question, addressed in recent years, is the definition of the limiting nuclearity above which clusters show properties characteristic of the extended state. This question has often been posed in terms of the density of electronic states. In this paper we pose the question in terms of the coupling between vibronic states for small metallic clusters and we take as our diagnostic the observation of delayed ionization following multiphoton excitation. This process involves a nonadiabatic coupling between potential energy surfaces and at the internal energies reached in this work occurs in competition with dissociation.

The competition between ionization and fragmentation following photoexcitation of small metal clusters is in some sense a central issue for many of the current experimental methods involving metal cluster beams. This is because these cluster beams are usually interrogated using an ionization, more specifically a photoionization, detection scheme. Whenever possible, the photoionization wavelength is selected to be just above the photoionization threshold of the species of interest in order to favor ionization over fragmentation. However, for clusters with ionization potentials greater than 6.2 eV, this is often not possible nor convenient and in these circumstances multiphoton methods have been used. In such cases, there is the possibility that dissociation of the neutral cluster or the cluster ion can compete with ionization. In this paper we reexamine the question of the mechanism of multiphoton ionization and competition

between ionization and dissociation processes from the point of view of small clusters of the refractory, early transition series elements: niobium, tantalum, and tungsten. These elements have high work functions and heats of evaporation, and their clusters are thought to be strongly bound. As a consequence of this strong binding, we are able to observe delayed ionization in competition with dissociation for clusters vibronically excited beyond their ionization potential. We regard the delayed ionization process as the analogue of the process of thermionic emission of electrons observed for macroscopic sized samples of these materials. Just as the high heat of evaporation, in respect to the work function, ensures that these materials are suitable materials from which to construct electron emission filaments, the strong binding energy of the particular clusters involved ensures that they will show the phenomenon of delayed ionization in competition with dissociation.

The development of the chemistry of niobium clusters parallels the general development of metal cluster beam science.[2-27] This is because niobium has proven an ideal element with which to demonstrate aspects of metal cluster beam technology. It is easily vaporized using laser vaporization methods and readily forms clusters of high nuclearity. It has only one naturally occurring isotope and is ideal for mass spectroscopy. As the ionization potentials of all but its smallest clusters lie in regions of the spectrum readily accessible to conventional lasers, it has proven an ideal element for photoionization mass spectroscopy. Detailed threshold photoionization measurements have been made and ionization potentials for Nb_2 to Nb_{76} have been reported.[5,15,16]

Recently, the binding energies for Nb_2^+ to Nb_6^+ have been determined using collision-induced dissociation of niobium cluster beams in a guided ion beam mass spectrometer.[23-25] The primary dissociation pathway at low collision energies is atom loss; at higher energies, sequential atom losses occur. As both the cluster ionization potentials and cluster ion binding energies have been measured, the binding energies of neutral clusters could be derived. The observation that the atom binding energies for both the neutral and positively charged clusters are in the range 5 to 6 eV is consistent with the fact that niobium metal possesses one of the largest cohesive energies of all elements.

The proposition that niobium clusters are strongly bound, while reasonable, is in some disagreement with the work of Cole and Liu.[26] These authors studied the metastable decay of niobium cluster ions induced by multiphoton absorption. They invoked the concept of "clusters within a cluster" to explain various experimental results.[26,27] While this concept is not fully defined, it is hard to imagine that niobium clusters will agglomerate via weak van der Waals bonds without forming a single strongly bound cluster. It was partly to resolve this dichotomy that the present work was performed. In brief, we believe that the results of Cole and Liu have been misinterpreted and that the metastable ion peaks arise from delayed ionization of neutral clusters and not from secondary dissociation of cluster ions.

II. EXPERIMENT

A metal cluster beam apparatus with a Smalley-type metal cluster source[28] and time-of-flight laser photoionization and electron spectrometers as diagnostics was used. The time-of-flight mass spectrometer (TOFMS) is somewhat unconventional in that it is in line with the direction of the metal cluster beam. The in-line geometry ensures that the cluster ions are accelerated collinearly with the neutral beam, unlike many other beam machines which accelerate the ions perpendicularly. The collinear design has an advantage in that there is no "mass window" effect. All ion masses produced get to the detector with equal efficiency. The perpendicular design requires an electrostatic deflection field to be scanned in order to see the whole cluster ion distribution.

The apparatus is shown schematically in Fig. 1. The cluster growth region is typically 14 cm long. The distance from the exit of the growth channel to the skimmer (Beam Dynamics Inc., 2 mm orifice) is 12 mm. A pair of deflection plates is positioned immediately after the skimmer to remove any ions produced in the source from the beam. These plates were found to be necessary for high resolution mass and photoelectron spectroscopic work. The distance from the point of vaporization to the point of ionization is 64.5 cm

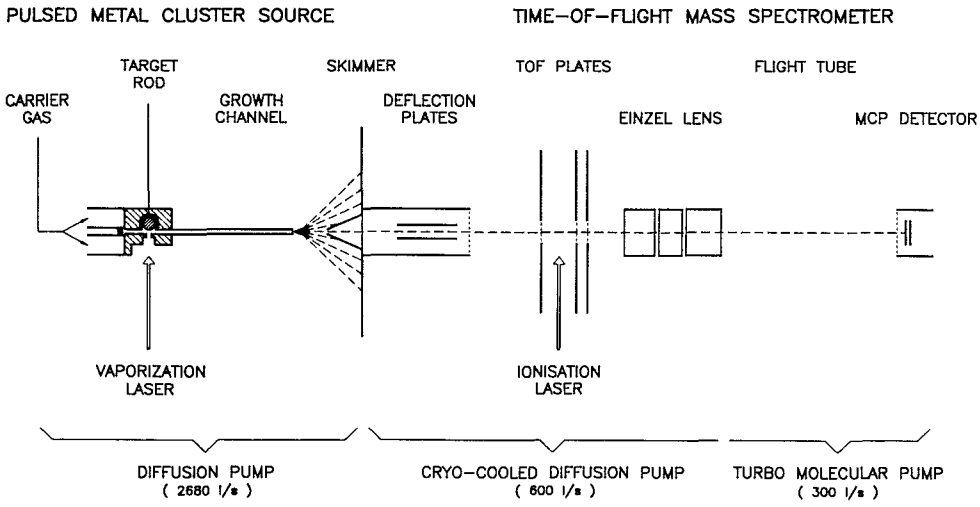

FIG. 1. The metal cluster beam and in-line time-of-flight mass spectrometer. An electron detector views the ionization region along an axis perpendicular to both the molecular and laser beams and is not shown in this diagram, see text. (TOF: Time-of-flight; MCP: Microchannel plate).

and the distance from the point of ionization to the microchannel plate detector is 165.4 cm. One problem with the in-line design was due to the direct line-of-sight from the source to the ion detector. This resulted in an intense signal due to light from the vaporizing laser and plasma. This was eliminated by allowing a small curve in the cluster building channel which effectively absorbed the light flash, but allowed the gas mixture to pass unimpeded.

The clusters are ionized by a laser beam which passes midway between the first and second TOFMS plates.The wavelengths used to ionize the clusters were either 308 nm (XeCl excimer laser, Lumonics TE-860), 351 nm or 248 nm (XeF or KrF excimer laser, Lumonics Excimer-500), or 220 nm (frequency doubled, in BBO, excimer-pumped-dye laser, Lumonics Hyperdye-300). As the excimer laser wavelengths drive multiphoton ionization processes, great care was taken to ensure that the spatial intensity profiles of their beams were well defined and uniform. The excimer laser beams were attenuated before being passed through simple spatial filters. The beams were expanded and collimated and a reasonably homogeneous portion of the beam intensity was selected using an aperture. They were then reflected from beam splitters and passed through the second chamber parallel to the plates of the TOFMS. The frequency-doubled dye laser is used to drive one photon ionization process and the requirement for spatial uniformity is fortunately less severe. The dye laser beam was expanded and collimated and passed through an iris to select the most homogeneous part of the beam. This beam then passed through the second chamber collinear with the excimer laser beam. By selectively blocking these beams,we could rapidly change ionization wavelength and observe the effect on the mass spectrum under the same source conditions.

The spacing between the first and second plates of the TOFMS is 4.5 cm and is 1.5 cm between the second and third. A simulation of the electric fields between the plates and surrounding chamber using the SIMION simulation computer program has shown that the field between the plates is uniform with negligible curvature.[29] The ion acceleration field could be switched on rapidly, providing a pulsed mode of operation. This was achieved by holding the first plate at the same voltage as the second plate until the TOFMS was required. Then the first plate could be pulsed up to the normal operating voltage by capacitively coupling the switched output (Directed Energy Inc. model HV1000) of one of the high voltage supplies. It was possible to generate a true square wave pulse of a few hundred volts with a rise time of less than 50 ns and a duration of over 20 μs. The TOFMS voltages in both pulsed and DC mode were adjusted to give optimal space focusing,[30] as judged by the width of the Nb_7^+ peak observed following photoionization at 220 nm. Typically, the middle plate, spaced by 1.5 cm from the grounded plate, was held at + 1070 V. The first plate was held at + 1250 V for DC operation and was held at + 1070 V and was pulsed to + 1250 V during pulsed operation. The resolution of our mass spectrometer under these conditions was approximately 700 [flight time/full width at half maximum (FWHM) Nb_7^+] as is shown in Fig. 2.

The signal from the detector was passed into an amplifier (LeCroy model 6102) and a transient recorder (LeCroy model TR8818), which has a maximum sampling rate of 100 MHz. To improve the signal-to-noise ratio, we would typically sum 1000 or 4000 mass spectra.

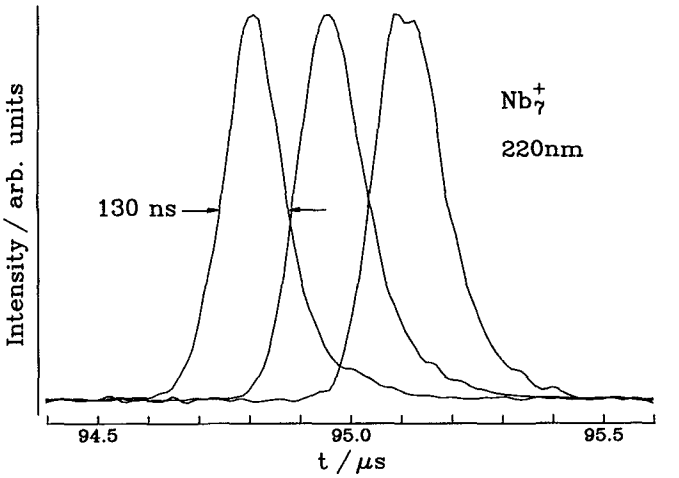

FIG. 2. The effect of the neutral cluster's velocity upon the mass spectrometer transit time. This effect is a direct consequence of the in-line arrangement shown in Fig. 1. The three data sets were obtained at delay times between the vaporization and ionization (220 nm, 100 μJ cm^{-2}) lasers of 420, 470, and 510 μs, respectively. This figure also illustrates that the effective mass resolution of the TOFMS is approximately 700. Peak heights have been normalized.

Photoelectrons are detected in a plane orthogonal to the cluster and laser beams by a second time-of-flight spectrometer and microchannel plate arrangement which is not shown in Fig. 1. This required that the ion TOFMS plates were grounded. A positive bias of 115 V, applied to the front plate of a microchannel plate electron detector mounted about 11 cm above the ionization region, ensured that electrons were detected with flight times of around 110 ns independent of their initial energy or direction. This arrangement did not give uniform extraction fields for the passage of electrons to the detector in consequence of the low voltages used and the proximity of the ground planes of the TOFMS electrodes. As a result, the time resolution of the electron spectrometer in this configuration was less than ideal (minimum peak width was around 90 ns). However, it was sufficient to confirm the production of delayed photoelectrons whenever the cluster mass spectra peaks were tailed. Following this confirmation, the electron spectra were repeated by removing the in-line TOFMS electrodes from the second chamber and inserting a photoelectron spectrometer. This spectrometer was essentially the simple, cross beam, space focused, two plate TOFMS which we have described in a previous publication.[31] Field simulations showed its collection efficiency to be close to unity. Its time resolution proved ideal, peak widths as narrow as the laser pulse, 14 ns, could be observed. All photoelectron production profiles presented in this paper were measured using the second arrangement.

One consequence of the linear TOFMS geometry is that the effect of changing source conditions on the cluster intensity and velocity distributions can be rapidly assessed. It was found that the observed cluster mass spectrum was depen-

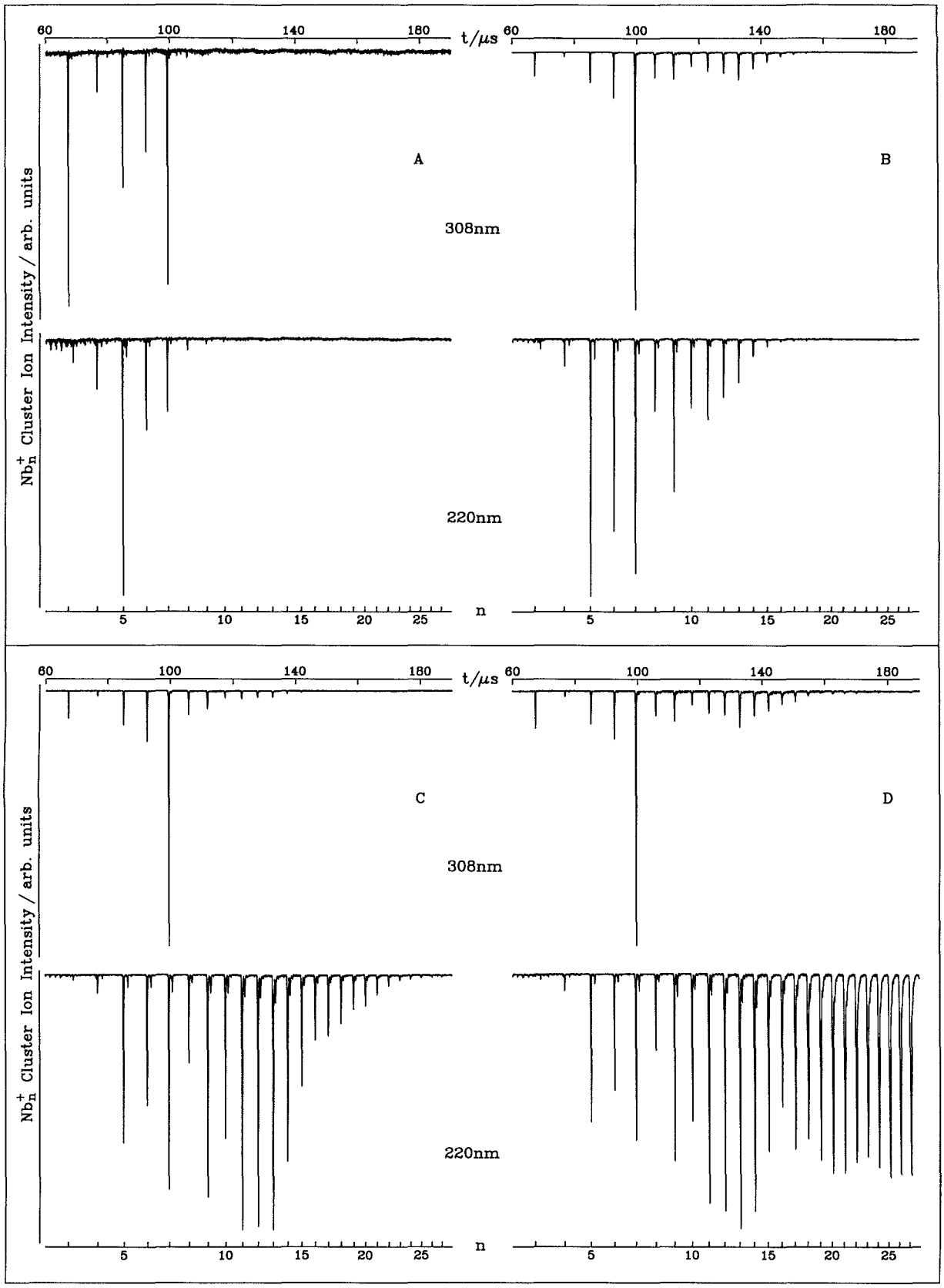

FIG. 3. General features of the direct (220 nm, 140 μJ cm^{-2}) and multiphoton (308 nm, 550 μJ cm^{-2}) ionization of niobium clusters. The data were obtained as a function of delay time between the vaporization and ionization laser pulses of 500 (A), 520 (B), 540 (C), and 570 (D) μs respectively. A pulsed extraction field delayed by 4.5 μs from the ionization laser was used to integrate the ionization signals; peak shapes in this figure do not reflect the ionization decay dynamics. Note (i) the mass-dependent velocity slip apparent for large clusters; (ii) the loss of high mass cluster peaks in the 308 nm data; and (iii), the correlation between the intensity of specific cluster masses in the 308 and 220 nm data.

dent upon both the time of firing of the vaporization laser with respect to the gas pulse and the timing of the ionization laser with respect to the vaporization laser. The former dependence is expected in terms of an optimal gas pressure to promote cluster building. The latter effect, which is illustrated in Fig. 3, indicates that there is a considerable mass-dependent velocity slippage for the niobium clusters in the expansions used in this study. This effect is important to the current work as it allows a convenient access to different cluster distribution patterns prior to ionization. Thus, by adjusting the firing time of the ionization laser to interact with the front of the cluster pulse we may excite a distribution of light clusters; whereas by firing the ionizing laser later in the pulse we may interact with a distribution of larger clusters.

The mass-dependent slippage in arrival time of the heavier clusters at the ionization region can have several contributing factors. Heavier clusters may acquire lower velocities in the supersonic expansion, a true velocity slippage effect, or larger clusters may exit the cluster building tube later in time than smaller clusters do. The in-line geometry allows these two factors to be addressed independently. This is because the flight time of ionized clusters from the ionization region to the MCP detector is explicitly dependent upon the neutral cluster's velocity prior to ionization. As the cluster's velocity can be calculated, its exit time from the cluster tube can be determined and the kinetics occurring within the cluster building region can be addressed. We intend to report upon this approach to clustering kinetics and cluster reaction kinetics in a future publication. For the present, we note that the results of Fig. 2 illustrate the effect. The flight time of the Nb_7^+ ion through the mass spectrometer is shown to shift later in time as the time of firing the ionization laser is delayed. Knowing the exact dimensions of the mass spectrometer, the field strengths, and the precise mass to charge ratio for Nb_7^+, we may solve for the cluster velocity. Velocities of 1470, 1370, and 1290 ms^{-1} are obtained. Solving for the exit time from the cluster tube, we find that these particular Nb_7^+ velocity groups exited the cluster building tube within 41 μs of each other.

There is another phenomenon that should be discussed and that surrounds the observation of cluster oxides and carbides. All reported mass spectra of niobium clusters show some evidence for small monoxide and dioxide peaks accompanying the bare metal cluster peaks.[2-4,9,10,14,17-21,25,26] These are due to impurity effects. There are two potential sources, the helium carrier gas and the surface of the metal rod. We have gone to great lengths to purify the helium used in this work, but still oxide peaks remain. The high resolution (the leading superscript indicates the photoionization wavelength) mass spectrum shows that these cluster monoxide, Nb_nO^+ peaks are often accompanied by cluster carbide peaks, Nb_nC^+. However, we have found that the simple expedient of stopping the rotation of the metal rod attenuates these peaks rapidly. When the rod is stationary, the laser ablates and removes a surface layer containing impurities derived from the ambient vacuum. When the rod rotates, the time between laser pulses falling on any particular spot is far greater and the impurity layer has time to reconstitute. Experiments in which a 10^{-3} dilute mixture of deuterium in helium is passed over the metal rod during laser ablation and then replaced with pure helium, show that deuterated niobium clusters are also produced by this surface impurity incorporation/ablation mechanism. We intend to report further on these effects in a future publication. For the time being, we note that whenever it was of importance to examine the decay of niobium cluster peaks, avoiding the influence of impurity peaks, the rod rotation was stopped or the surface of the rotating rod was extensively pretreated by exposure to the ablation laser. When the rod is stopped, however, the observed cluster distribution gradually changes as the ablation kinetics and subsequent clustering are affected by the changing surface morphology as the ablation proceeds. Consequently, the length of signal averaging acquisition was limited in this mode of operation. Whenever it was intended that the oxide peaks were the object of study, a 10^{-4} dilute mixture of oxygen in helium was used. When it was intended to study carbides, a 10^{-5} dilute mixture of propane in helium was used. Figure 4, which shows the mass spectrum obtained using pure helium carrier gas with the rod rotating and the spectra obtained with the dilute oxygen and propane mixtures, illustrates these effects.

III. RESULTS

The three refractory elements niobium, tantalum, and tungsten have been found to respond in similar ways to the experiments carried out in this study. In presenting the results, we have chosen to emphasize results obtained with niobium as these results are at times in disagreement with those of Cole and Liu.[26] However, we also present specific aspects of the results obtained with tantalum and tungsten where these are interesting and warranted.

A. Direct-*v*-multiphoton ionization

1. Correlation between mass spectra at different wavelengths

Figure 3 was discussed in the experimental section as exemplifying the velocity slippage effect which allows us to probe different cluster distributions simply by varying the delay time between the vaporization and ionization laser pulses. This aspect can be most readily appreciated by considering the results obtained at 220 nm. This wavelength corresponds to 5.63 eV which is above the ionization potential of all niobium clusters with the exception of Nb_2 (6.2 eV), Nb_3 (5.81 eV), and Nb_4(5.64 eV).[16] Thus, we expect the ionization of niobium clusters of higher nuclearity than the tetramer to be direct one photon processes at this wavelength. We have confirmed that the intensities of such cluster ion peaks are linearly dependent upon the 220 nm beam fluence and take this to mean that the intensity of the Nb_n^+ peaks in the 220 nm spectrum is directly proportional to the concentration of niobium clusters, Nb_n, on the beam.

It is important to note that the data presented in Fig. 3 were obtained using the pulsed extraction field delayed by 4.5 μs from the ionization laser pulse. In consequence, the peak shapes do not represent the ionization dynamics. Instead, they represent the integrated ionization yield. It is also

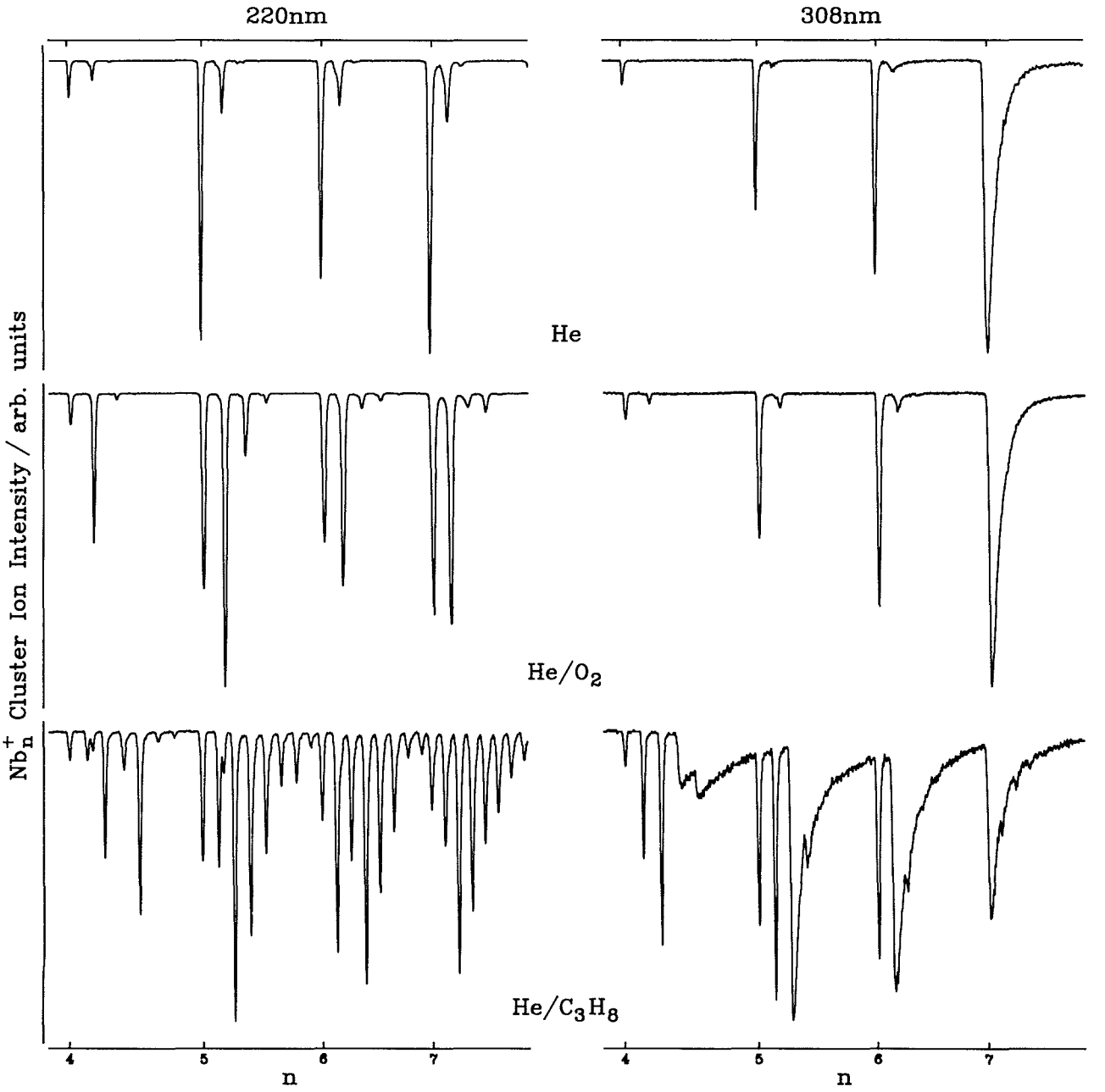

FIG. 4. Plasma chemistry for niobium clusters. This figure compares the mass spectra observed with pure helium carrier gas (top panel), a 5×10^{-4} dilute mixture of oxygen in helium (middle panel) and a 10^{-4} dilute mixture of propane in helium (bottom panel). The laser fluences were 150 μJ cm^{-2} (220 nm) and 900 μJ cm^{-2} (308 nm). The production of derivatized oxide and carbide clusters is revealed by the 220 nm data. Note that (i) the oxides are essentially absent in the 308 nm data, whereas the carbides are present; (ii) there is a strong nuclearity effect revealed in the decay times of the cluster carbide peaks.

important to note that all mass spectra presented in this paper are normalized to the height of the most intense peak displayed in the figures.

A more salient feature of Fig. 3 is shown by the 308 nm data. Only smaller cluster ions are observed. Peaks for Nb_3^+ to Nb_7^+ appear to be relatively strong in comparison to peaks for Nb_8^+ to Nb_{18}^+. Peaks above Nb_{18}^+ appear to be absent. The data in Fig. 3 do show that the (308 nm, Nb_n^+) peaks are proportional in height to the (220 nm, Nb_n^+) peak heights obtained under otherwise identical conditions, although this point may be obscured to some degree by the normalization procedure. This point is made more forcefully in Fig. 5, which shows the linear correlation between the absolute intensities of 308 nm, Nb_n^+ and 220 nm, Nb_n^+ for data obtained over a wide range of delay times between the vaporization and ionizing lasers, and hence widely varying cluster distributions. This figure shows that the 308 nm, Nb_n^+ peaks are derived from Nb_n precursors and not from fragmentation of a higher mass parent ions as suggested by Cole and Liu.[26] In clear contradiction with their mechanism, it is not possible to correlate a 308 nm, Nb_n^+ with a 220 nm, Nb_m^+ peak, unless n is equal to m.

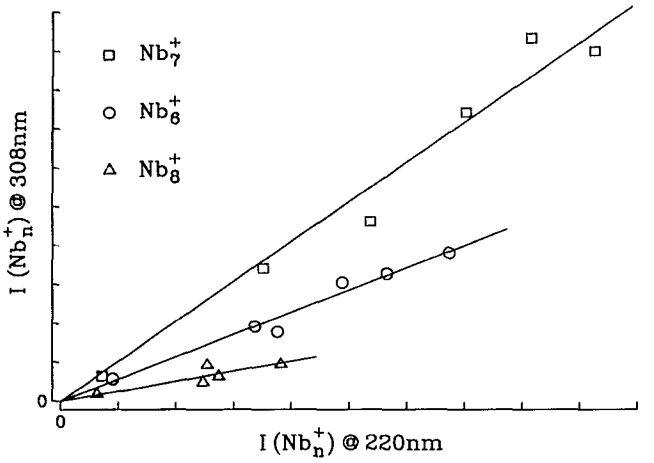

FIG. 5. Peak correlation diagram. This figure was derived from the data in Fig. 3. Different niobium cluster distributions were probed by varying the delay time between the vaporization and ionization lasers (in consequence of the cluster size-dependent velocity slip). The correlation implies that the 220 nm (direct) and 308 nm (multiphoton) ionization signals have common precursors. The intensity of 308 nm, Nb_6^+ has been multiplied by 2 for clarity of presentation.

2. Laser fluence dependence

The wavelength 308 nm corresponds to 4.03 eV; thus, the 308 nm spectra must be due to multiphoton processes. This was confirmed by power dependence studies in which it was found that the intensity of 308 nm, Nb_n^+ peaks was not linear in the 308 nm laser fluence, ^{308}I. For instance, 308 nm, Nb_7^+ was proportional to $^{308}I^{1.95}$ in the fluence range 0.04 to 2.0 mJ cm^{-2} and 308 nm, Nb_3^+ was proportional to $^{308}I^{1.98}$ over the same range.

At 220 nm, the intensity of all mass peaks was linear in the 220 nm laser fluence.

B. Decay profiles of peaks in mass spectra

1. 308 nm mass spectra

In agreement with Cole and Liu, we find that peaks in the 308 nm photoionization mass spectrum are tailed.[26] In the low fluence range, the 308 nm, Nb_7^+ peak can be fit to a *single* exponential. These data are shown in Fig. 6. Accompanying the niobium data are equivalent data for 308 nm, Ta_7^+ and 308 nm, W_7^+. The solid curves are fits to the data of single exponential decays with decay times of 0.67 ± 0.02, 0.40 ± 0.01, and $1.54 \pm 0.07\,\mu$s for 308 nm, Nb_7^+, 308 nm, Ta_7^+, and 308 nm, W_7^+, respectively.

We find that the 308 nm, Nb_8^+, 308 nm, Nb_9^+, and 308 nm, Nb_{10}^+ peaks exhibit biexponential decay. The decay time of the fast component is limited by the time resolution of our spectrometer. This component could be due to a contribution from direct two-photon ionization at the laser fluences used to acquire the mass spectra. The decay times of the longer lived components are 3 ± 1, 4 ± 1, and $> 10\,\mu$s for 308 nm, Nb_8^+, 308 nm, Nb_9^+, and Nb_{10}^+, respectively.

2. The seven atom effect

One of the most intriguing results of this study is that the tailing in the 308 nm mass spectra shows a distinct seven

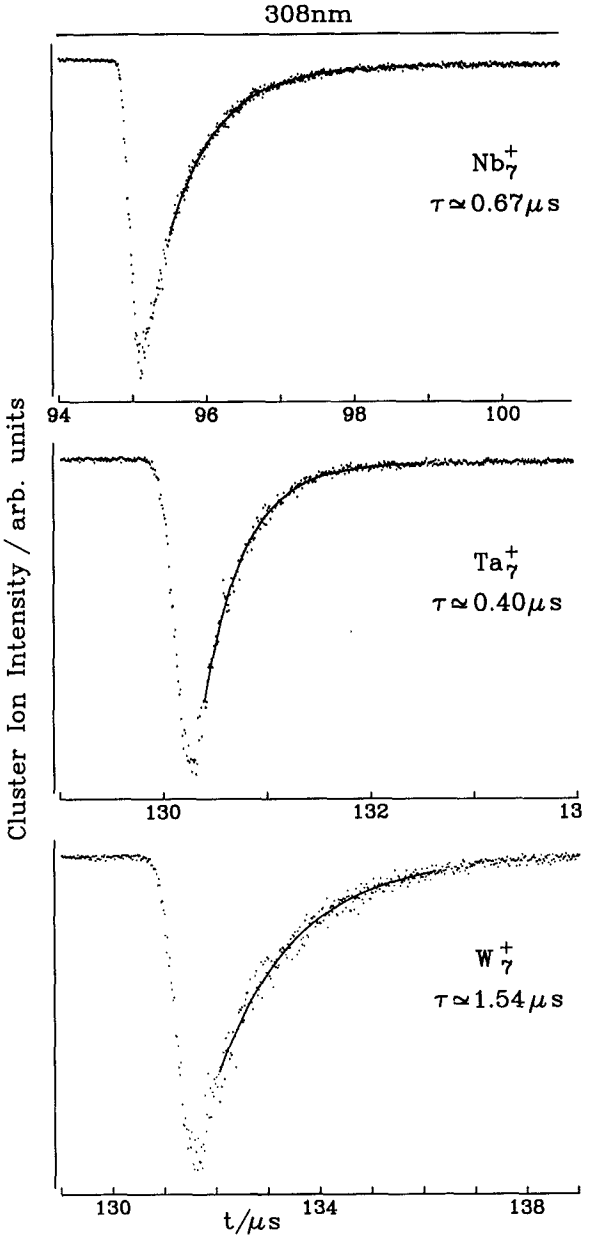

FIG. 6. An expanded view of the time dependence of the seven atom cluster peaks for niobium, tantalum, and tungsten clusters. The data were obtained at 308 nm (laser fluences of 0.9, 0.9, and 1.3 mJ cm^{-2} for niobium, tantalum, and tungsten, respectively); at 220 nm, the peaks were sharp. The solid line is a single exponential fit to the data. The fit was not carried out to earlier times because of the effect of the instrumental resolution, nor to later times because of the effect of time distortions as the clusters move through the mass spectrometer.

atom effect. This result was first noted by Cole and Liu who found that at 248 nm, the peaks due to Nb_7^+, Nb_6O^+, and $Nb_5O_2^+$ were all tailed; whereas, peaks of six atom clusters were not.[26] Cole and Liu attributed this effect to an effect of electronic or geometrical structure.[26] We disagree with this interpretation and believe that the effect has its cause in statistically determined rate processes, *vide infra*.

We find evidence for the production of cluster monoxides, dioxides, and trioxides using the dilute oxygen mixture as a carrier gas and an ionization wavelength of 220 nm, see Fig. 4. However, all of these oxidized cluster species are es-

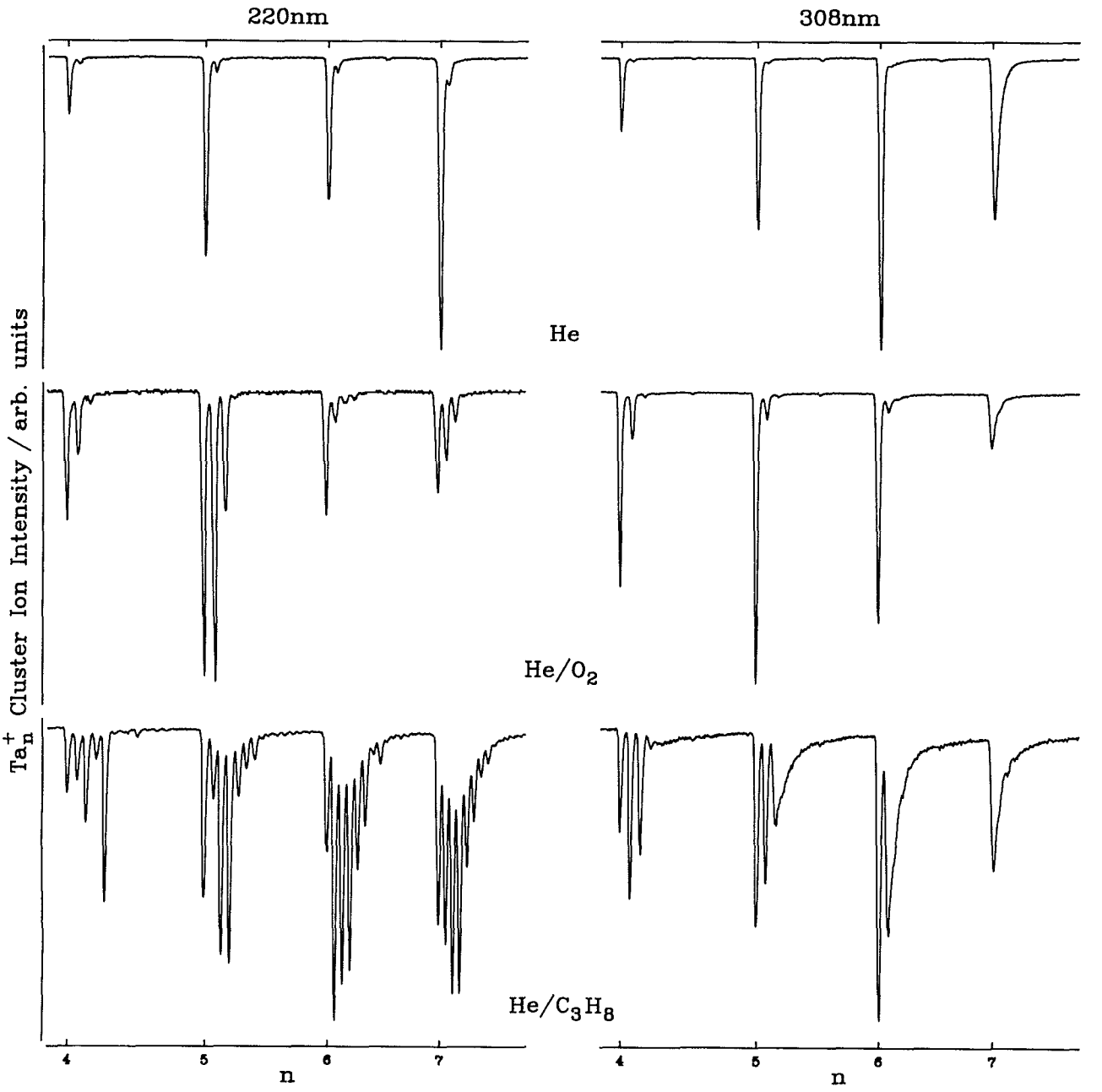

FIG. 7. Plasma chemistry for tantalum clusters (as for Fig. 4, niobium). The laser fluences were 190 μJ cm^{-2} (220 nm) and 1.4 mJ cm^{-2} (308 nm). A 2×10^{-5} dilute mixture of oxygen and a 3×10^{-5} mixture of propane in helium was used. Note the strong effect of nuclearity upon the decay times of tantalum carbide clusters.

sentially missing in the 308 nm spectra in which the bare cluster peaks dominate. In particular, no tailed peak is observed at Nb_6O. However, when the 10^{-4} dilute mixture of propane in helium is used, cluster carbide peaks, up to the tetracarbide, are observed in both the 220 and the 308 nm spectra. In particular, clusters with less than seven atoms (Nb_6, Nb_5, Nb_5C, Nb_4, Nb_4C, and Nb_4C_2) have sharp peaks; clusters with *exactly* seven atoms (Nb_7, Nb_6C, Nb_5C_2, and Nb_4C_3) have tailed peaks, with a decay time of approximately 1 μs; and, clusters with more than seven atoms (e.g., Nb_7C, Nb_6C_2, Nb_5C_3, and Nb_4C_4,) have long decay times and appear as steps in the mass spectrum, superimposed upon the falling edge of the seven atom peaks. This result is also seen in the equivalent tantalum spectra, as is shown in Fig. 7. The results for tungsten clusters are qualitatively similar, but are obscured by the large number of isotopomers.

3. Wavelength dependence of the peak shape

We find evidence for tailing of the mass spectrum peaks at other photoionization wavelengths. Figure 8 shows data obtained for niobium clusters at 351 nm (3.53 eV) and 248 (5.0 eV) in comparison with the 308 nm and 220 nm data already presented. The data obtained at 351 nm are interesting in comparison with the data at 308 nm. The 351 nm, Nb_7^+ peak is tailed and has a considerably longer decay time

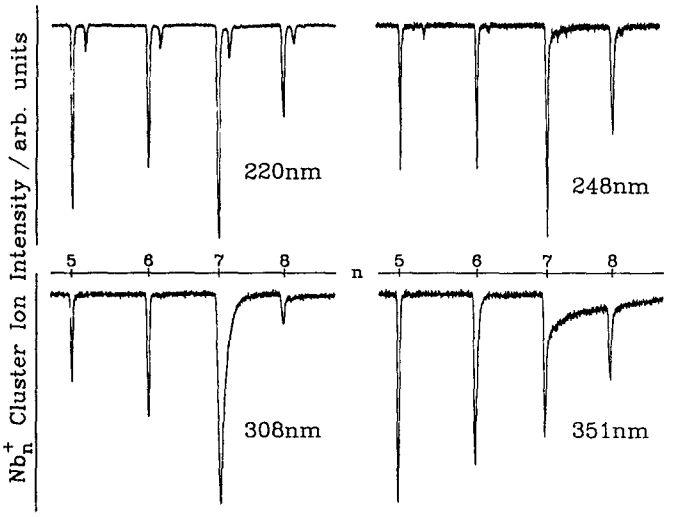

FIG. 8. Wavelength effects in the ionization of niobium clusters. The laser fluences were 170 μJ cm^{-2} (220 nm), 1.1 mJ cm^{-2} (248 nm), 1.3 mJ cm^{-2} (308 nm), and 1.2 mJ cm^{-2} (351 nm). Note the tailing observed on the 308 nm, Nb_7^+, 351 nm, Nb_6^+, and 351 nm, Nb_7^+ peaks. In particular, note the difference in peak width between the 308 nm, Nb_6^+ (instrumentation limited) and 351 nm, Nb_6^+ signals.

(5.5 ± 1.5 μs) than the 308 nm, Nb_7^+ peak; the 351 nm, Nb_6^+ peak is also tailed and has a longer decay time (0.19 ± 0.01 μs) than that of the 308 nm, Nb_6^+ peak which is limited by the resolution of the mass spectrometer. These observations will be shown to be quantitatively consistent with the statistical decay model presented below.

The 248 nm data are limited as 5.0 eV directly ionizes all niobium clusters larger than Nb_9 in a one photon process.[16] Thus, we are unable to observe the interesting two-photon processes for the larger clusters as any two-photon effects are masked by direct ionization at this wavelength. However, we have confirmed that the intensity of smaller cluster peaks is nonlinear in the 248 nm laser fluence.

4. Pulsed acceleration field experiments

The results of pulsed field experiments are presented in Fig. 9. This figure shows the effect of the delayed pulsed extraction field on the 308 nm, Nb_7^+, 308 nm, Ta_7^+, and 308 nm, W_7^+ peaks. The result is unequivocal: the effect of the pulsed field is simply to integrate the intensity of the ionization that occurs before the voltage pulse is applied. The data suggest that the precursor of the seven atom cluster ions is either a neutral cluster or a very large cluster ion. Taken with the peak correlation data shown in Fig. 5, the implication is that the precursor species are Nb_7, Ta_7, and W_7.

The interpretation of the pulsed field data given above is supported by the simulations shown in Fig. 10. Briefly, suppose that a cluster ion M_m^+ decays in a region of constant electric field to M_n^+ with unimolecular rate constant k_{true}. It is straightforward to show algebraically and to confirm with exact ion flight time simulations that the M_n^+ peak will be tailed to higher mass by an exponential decay due to the decay of M_m^+ into M_n^+ with an observed decay time, τ, given

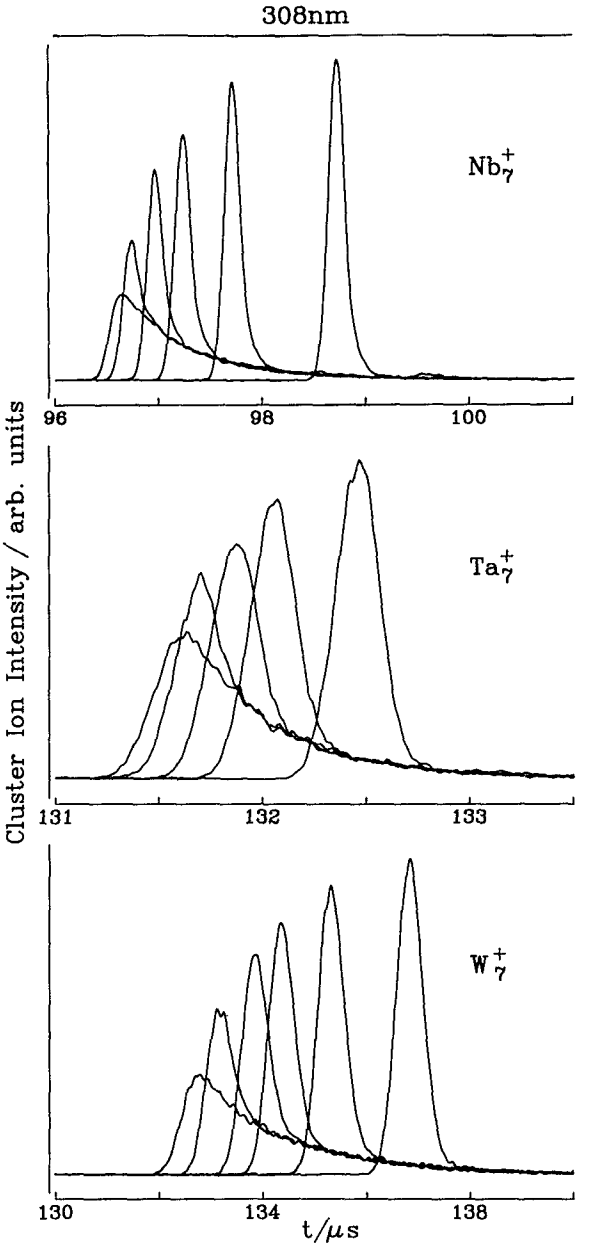

FIG. 9. Effect of pulsed extraction fields on the seven atom cluster decays at 308 nm. The laser fluence was 1.5, 1.2, and 1.3 mJ cm^{-2} for niobium, tantalum, and tungsten, respectively. The extraction field was 24 μs wide and was delayed with respect to the ionization laser (delay times: 140, 370, 650, 1120, 2110 ns, niobium; 120, 290, 470, 880 ns, tantalum; and, 440, 1170, 1670, 2640, 4140 ns, tungsten). Note that the delayed field integrates the prior ionization and that the signals overlap once the extraction field is applied. Peak areas have been normalized to remove the effect of slight fluctuations in source intensity.

by

$$\tau = 1/k_{\text{observed}} \approx (m-n)/(m \times k_{\text{true}}). \quad (1)$$

Figure 10 presents results of full simulations of the Nb_7^+ peak shape in a pulsed field experiment for various combinations of m and k_{true} which would, in combination, give the peak shape observed in a DC field. It can be seen that the fragmentation and fission precursors, Nb_9^+ and $Nb_{(15-30)}^+$, suggested by Cole and Liu, cannot fit our pulsed field data.[26]

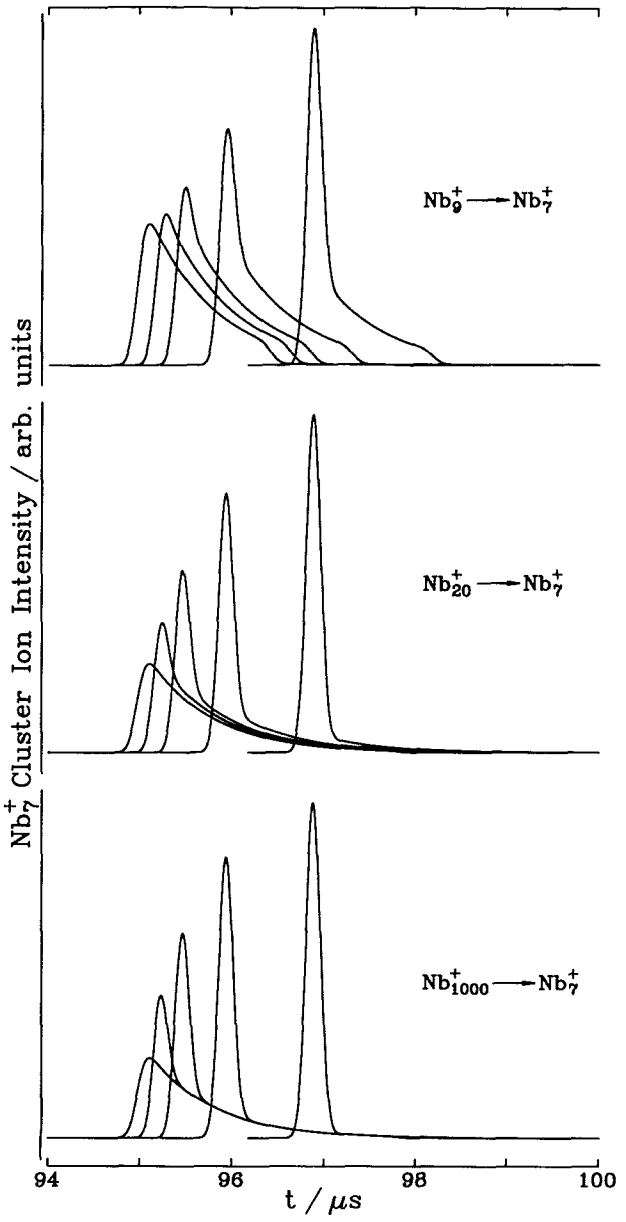

FIG. 10. Simulations of the metastable decay of niobium ions in a pulsed extraction field experiment of the kind shown in Fig. 9. The assumed decay rates were $3.11\times10^5\ s^{-1}$ for $Nb_9^+ \rightarrow Nb_7^+$, $9.8\times10^5\ s^{-1}$ for $Nb_{20}^+ \rightarrow Nb_7^+$, and $1.39\times10^6\ s^{-1}$ for $Nb_{1000}^+ \rightarrow Nb_7^+$. These rates were chosen to be consistent with an observed decay rate of $1.4\times10^6\ s^{-1}$; see Eq. (1) and Figs. 6 and 9. Pulsed field delay times of 250, 500, 1000, and 2000 ns were assumed. Note that for the light ion precursors, the tail of the decays do not overlap after the application of the pulse field in contrast to the data presented in Fig. 9.

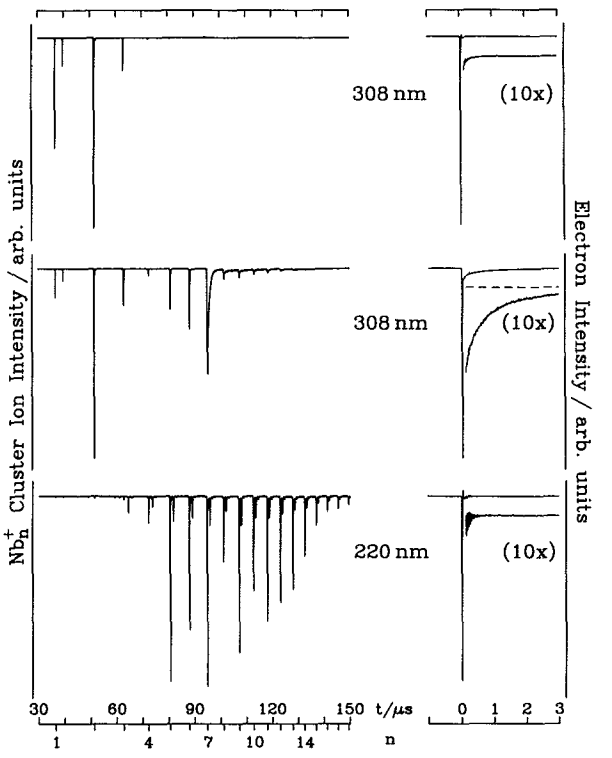

FIG. 11. Comparison of cluster mass and photoelectron peaks at 220 and 308 nm. For the top panel, the firing time of the ionization laser was chosen to excite a distribution of small clusters in order to minimize the contribution of tailed mass peaks ($n > 6$). For the other panels, the delay was adjusted to maximize the Nb_7^+ signal. In the 308 nm spectra, the Nb_2 peak is truncated. Fluences were 1.2/1.0 mJ cm^{-2} (308 nm) and 96/1.7 μJ cm^{-2} (220 nm) for the mass/photoelectron spectra. The dashed line indicates the baseline for the expanded photoelectron signal. Note the observation of delayed electrons whenever tailed ionization peaks are observed and the biexponential decay in the case of the Nb_8, Nb_9, and Nb_{10} mass peaks at 308 nm.

C. Photoelectron production time profiles

Figure 11 shows the form of the photoelectron time-of-flight spectrum in contrast to the time-of-flight mass spectrum observed under various experimental conditions. Two general comments on the photoelectron "spectra" are appropriate. Firstly, the photoelectrons observed derive from ionization of all clusters contributing to the mass spectrum. Secondly, when operated in this mode, the photoelectron spectrometer is relatively insensitive to the initial energies of the photoelectrons; the spectrometer more properly functions as a detector of the time-of-production of the photoelectrons. The time resolution of the spectrometer is good; peaks for photoelectrons produced at 220 nm, i.e., direct ionization, have a width of ≈ 14 ns. We have confirmed that the long lived photoelectrons produced at 308 nm are not the result of space charge effects by comparing results over a range of electron fluxes down to the few particles per pulse limit. Whenever the mass spectrum shows tailed ion peaks, the photoelectron peak shows an equivalent tailing reflecting a delayed source of photoelectrons, or a delayed ionization process.

D. The behavior of other elements

Figure 12 shows survey spectra for tantalum and tungsten at 220 nm and 308 nm in comparison with data for niobium. This figure is presented in order to emphasize the similarity of behavior among these three refractory elements. Other elements were surveyed but gave different results. Vanadium, indium, titanium, and cobalt gave cluster mass spectra at 220 nm, but vanadium, indium, and cobalt did not give mass spectra at 308 nm. A 308 nm, spectrum for titanium could be induced, but only at fluences more than an

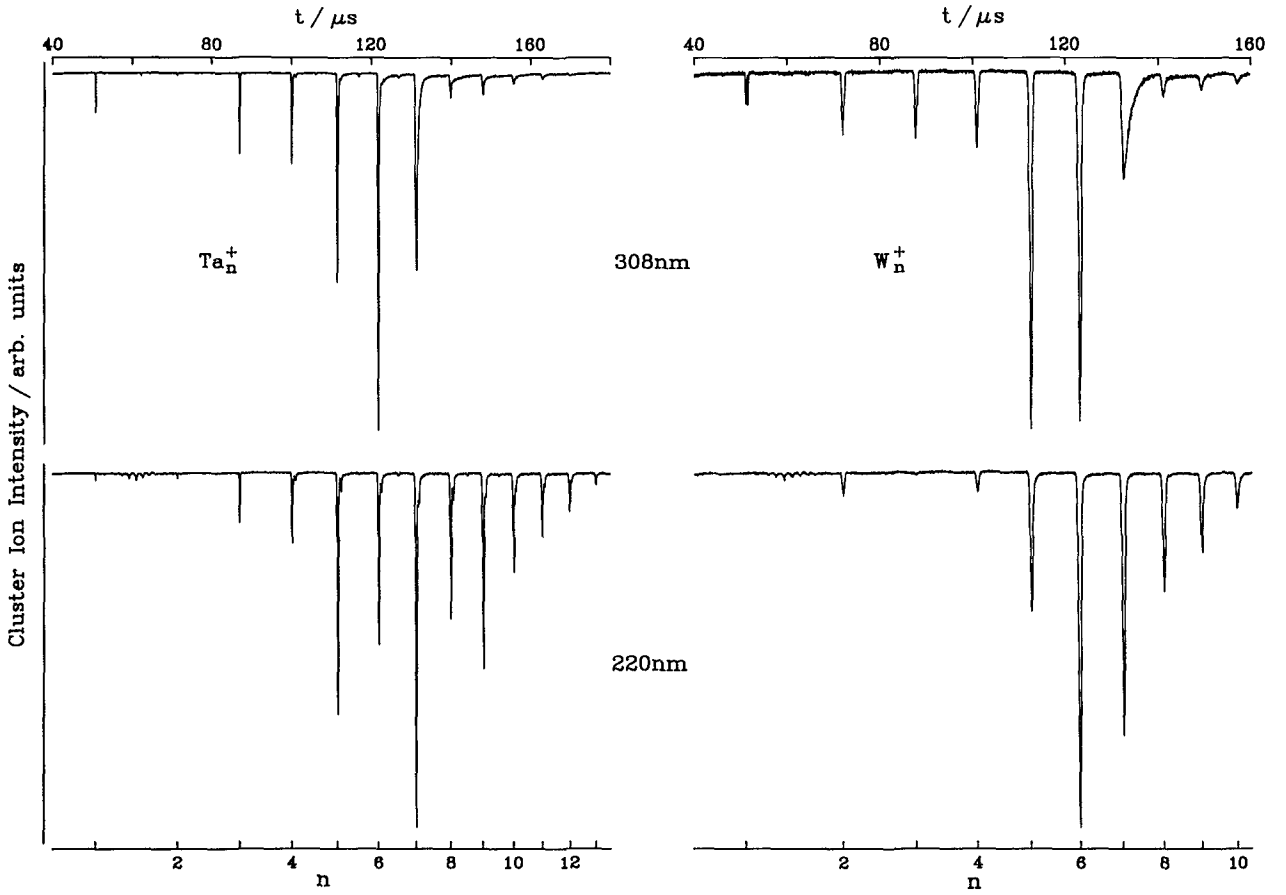

FIG. 12. General features of the direct (220 nm, 170 μJ cm^{-2}) and multiphoton (308 nm, 1.2 mJ cm^{-2}) ionization of tantalum and tungsten clusters.

order of magnitude greater than those used in the main body of this study.

E. A comparison with previous data

In this section, we summarize our results in comparison with the results obtained by Cole and Liu.[26]

We have studied the ionization of niobium, tantalum, and tungsten cluster beams at 220, 248, 308, and 351 nm. Cole and Liu used 193, 222, 248, 308, 351, and 620 nm. We find that whenever the photoionization laser energy is greater than the cluster ionization potential, the mass spectrum peaks are sharp. Cole and Liu report instances when this is not the case.[26]

Cole, Liu, and Riley found that the photoelectrons at 248 nm were produced in a single sharp peak of 30 ns width.[27] We would expect to agree with this observation, even though we have not confirmed it, as our 248 nm mass spectra are dominated by sharp peaks. However, at 308 nm, we find evidence for the production of delayed photoelectrons which correlate with the observation of tailed peaks in the mass spectrum.

We disagree on the form of the metastable decay of the Nb_7^+ peak. We find a single exponential decay which is longer at 351 nm than at 308 nm. The decay times in the Cole and Liu work are generally longer at 308 nm than at 351 nm. Cole and Liu find a decay which they fit to three components;[26] a fast component with time response limited by the resolution of their mass spectrometer and two slower components. They attributed these components to direct multiphoton ionization, cluster ion fragmentation, and cluster ion fission.

Potentially, the differences in results between the two studies can be attributed to differences in laser intensity and beam homogeneity. It is possible that their results were obtained at considerably higher fluences than were ours, either as a consequence of a less homogeneous spatial profile of the laser intensity or simply as a consequence of a greater laser pulse energy. In support of this suggestion, we have found that faster components enter into the 308 nm, Nb_7^+ peak shape whenever the beam intensity is increased or whenever an inhomogeneous beam is used. We attribute these effects to higher order processes which we will discuss below in terms of the ladder model. For the time being, we note that this work is concerned with two-photon processes which are observed at low laser fluences.

Cole and Liu suggested that the tailing on the niobium peaks observed in their experiments was due to unimolecular decay of higher mass cluster ions in the acceleration region of the mass spectrometer.[26] This is the standard explanation for metastable peaks in mass spectroscopy,[32] but we do not believe that this is the pertinent explanation in the present case. In contrast, we find that a pulsed extraction field merely integrates the exponential decay; this, together with the observation of delayed photoelectrons, strongly suggests a

delayed ionization channel. Metastable unimolecular decay of cluster ions within the acceleration region is plausible and is discussed under the ladder model below. However, an additional process, delayed ionization, is consistent with all of our observations and many of those of Cole and Liu.[26]

Cole and Liu postulated the concept of "clusters within a cluster" to explain certain of their observations. Among these is the observation that the extent of tailing as compared to the intensity of oxide peaks was dependent upon the source pressure.[26] We have searched for this effect, but have not observed it in the range of source pressures from 10 to 100 psi, nor do we find any substantial difference in the 308 nm, Nb_7^+ peak shape when argon is used as a carrier gas instead of helium. We do note that the intensity of cluster oxide peaks is somewhat variable and source dependent, *vide supra*, and this might have contributed to their observation. Another observation that was explained within the "clusters within a cluster" framework was the low translational energy of the cluster ions. This could not be fit by any plausible unimolecular rate theory.[26] We note that our proposal of delayed ionization does not require the ions to gain translational energy. Indeed, they should not.

Finally, Cole and Liu carried out some intriguing optical double resonance experiments which pointed out the involvement of long lived neutral states produced following the absorption of one 248 nm photon.[26] Whether these states are also involved prior to the ion decay process is not clear from their discussion.[26] It is possible that the decay time they report, 3.15 μs, may be due to passage of neutrals through the laser interaction region; at a velocity of 1.5 km s^{-1}, a laser beam diameter of 5 mm would be consistent with this. Nonetheless, it is just these long-lived neutral states which are central to our discussion of the mechanism behind the intriguing effects that are reported upon in this work.

IV. DISCUSSION

In this section, a model to account for the observations reported above is presented. The rates for dissociation and delayed ionization are estimated using statistical theory and are compared to the experiment. A ladder model, which might be operative at higher laser intensities, is considered. Finally, estimates are provided for the ionization and dissociation rates based solely upon known properties of bulk niobium.

A. A mechanism for two-photon ionization of refractory clusters

A model for the dynamics which are responsible for the observations described above has been given in an initial communication describing this work.[33] In this model, we distinguished between two types of ionization processes: Direct ionization and delayed ionization. We mean by direct ionization that optical excitation directly transfers energy to a single electron so that it is excited beyond the ionization potential and is therefore unbound. We understand the process of delayed ionization to involve the coupling of the cluster's vibronic energy so that a single electron reaches an unbound level. Central to this picture of the delayed ionization process and central to our concept of the photoexcitation mechanism is a description of the electronic manifold of a small metal cluster in terms of the nature of its electronic states, the nature of the coupling between them, and the nature of the electronic excitations.

The model involves the following steps:

$$M_n + h\nu_L \rightarrow M_n^* \tag{2}$$

$$M_n^* \rightarrow M_n^\dagger, \quad k_{\text{relaxation}}, \tag{3}$$

$$M_n^* + h\nu_L \rightarrow M_n^+ + e^- \tag{4}$$

$$M_n^\dagger + h\nu_L \rightarrow M_n^{\dagger *} \tag{5}$$

$$M_n^{\dagger *} \rightarrow M_{n-1} + M, \quad k_{\text{dissociation}}, \tag{6}$$

$$M_n^{\dagger *} \rightarrow M_n^+ + e^-, \quad k_{\text{ionization}}. \tag{7}$$

This mechanism provides the simplest set of equations with which to rationalize the results of our study and is applicable to those situations in which the photon energy, $h\nu_L$, is less than the ionization potential of a particular metal cluster M_n. The first process, Eq. (2), represents the photoactivation of M_n to produce an excited electronic state, M_n^*. Equation (3) represents the intramolecular relaxation of the electronic excitation over the vibronic levels of the cluster. The extent of this relaxation is not known *a priori*, but two consequences are recognized in this mechanism. In the first, Eq. (4), an electronically excited state absorbs a second photon such that the electronic excitation is greater than the ionization potential and prompt ionization results. This process is represented in Eq. (4) as proceeding from the initial excited state reached via Eq. (2), but there is no reason why other electronically excited states reached by processes akin to Eq. (3) could not be involved. The second consequence of Eq. (3) is recognized in Eq. (5). Here, a vibrationally excited metal cluster is excited such that the initial degree of electronic excitation is less than the ionization potential. Ionization can then only result from a nonadiabatic relaxation process represented as Eq. (7). As the vibronically excited metal cluster, $M_n^{\dagger *}$, has acquired from 7 to 10 eV internal energy through the absorption of two laser photons, the ionization process must compete with the process of dissociation, represented as Eq. (6).

The processes represented by Eqs. (2) and (4), taken together, represent the process of direct two-photon ionization. The extent of this process depends upon the competition between processes (3) and (4) which depends upon the laser *intensity*. Direct two-photon ionization should dominate the initial excitation mechanism at high laser intensities. At the lower laser intensities used in this work, we submit that Eq. (3) can compete with Eq. (4). The laser pulses used in this work are typically of 15 ns duration which requires that the rate of intramolecular relaxation, $k_{\text{relaxation}}$, is greater than 7×10^7 s^{-1}.

The experimentally observed decay time, τ, of an Nb_n^+ peak is given within the constraints of this model as

$$\tau = 1/k_{\text{observed}} = 1/(k_{\text{ionization}} + k_{\text{dissociation}}). \tag{8}$$

Moreover, we define the yield of ionization, Φ_I, as

$$\Phi_I = k_{\text{ionization}}/(k_{\text{ionization}} + k_{\text{dissociation}}). \tag{9}$$

Clearly, for ionization to be observed, $k_{\text{ionization}}$ must com-

pete with $k_{\text{dissociation}}$, although it need not be rate determining.

There are many precedents for vibrationally induced ionization throughout chemistry. These are analogues to the process of delayed ionization that we have suggested in our model. Among these are the vibrational autoionization of Rydberg states of neutral diatomic[34] and polyatomic molecules[35] commonly encountered in spectroscopic studies of highly excited electronic states. These processes are of importance in chemi-ionization reactions and following charge neutralization reactions between cations and either electrons or anions. An analogous process is electron autodetachment from negative ions. Brauman and co-workers clearly showed that this process could be induced by vibrationally exciting the ground state of an anion in a mass spectrometer using photons from a carbon dioxide laser and that electron detachment could proceed in competition with the absorption of infrared photons and with the dissociation of the anion.[36] Autodetachment of negative ions has also been proposed to account for the lifetimes of anions formed following electron capture by neutrals.[37,38] In that model, a simple statistical picture of the nonadiabatic, vibrationally induced electron detachment mechanism was developed. Finally, an important and seminal example of a vibrationally induced nonadiabatic ionization should be mentioned. This concerns the thermal dissociation of alkali halides following vibrational excitation in shock tubes. Dissociation to both neutral and charged atomic states was observed and the importance of nonadiabatic effects was clearly delineated.[39]

B. Discussion of rate processes

1. Excitation and relaxation

In principle, one might expect a smooth transition in the description of the electronic energy levels of a metal cluster from a homonuclear metal dimer, which can be understood in terms of discrete states coupled together by well characterized matrix elements to the extended metallic state which is characterized by collective excitations and by a continuum of electronic states, best discussed using translational symmetry and **k** space.[40] Viewed from the extended metallic state, there should equally well be a transition region in which the confinement of the electron gas, in an ever decreasing cluster size, gives rise to discrete, observable, quantized energy levels and "quantum size" effects.

The electronic structure of small clusters of alkali metals is perhaps the best understood of all classes of metallic elements. Nonetheless, the transition region discussed above is not yet well defined. Wigner and Seitz first proposed that electronic cohesion in these metals could be explained in terms of a free electron model in which electrons were confined in a spherical box.[41] This suggested the jellium model for small clusters of alkali metals in which all s electrons are confined in a spherical or uniaxial ellipsoidal well potential. The electron shells, defined by a principle quantum number n and an angular momentum quantum number 1, and their closing then determine the majority of the electronic properties of smaller alkali metal clusters.[42–44] The photoexcitation of larger alkali metal clusters can be understood in terms of a collective excitation of the valence electrons against the positive background of the ions.[45] Using modified Mie theory and a Drude free electron model, it is possible to calculate the spectrum of these "surface plasmon" resonances. They are predicted to red shift and broaden from the bulk values as the cluster size decreases, a consequence of an increase in molecular polarizability due to the spill out of electron density beyond the jellium potential wall,[46] and a decrease in the electron mean free path with respect to the collision frequency of the conduction electrons.[47] Observations of the electronic spectra of larger alkali clusters and cluster ions are generally consistent with this completely delocalized description of the electronic structure of alkali metal clusters.[43,47] However, the spectra of Na_3, Na_4, and Na_8 are highly structured and neither the continuum model nor the jellium model may be applicable at this size range.[47] It has been suggested that in this size regime, a molecular orbital approach may be more relevant.[47–49]

The decay of surface plasma oscillations into purely thermal motion is a topic of great interest in modern physics. Mechanisms such as Landau damping (coupling to electron hole pairs), coupling to shape fluctuations, and coupling to phonons have been discussed.[50] However, no measurements on small metal clusters have been made. Measurements of the surface plasmon decay time and the electron–phonon relaxation time for noble metal films, though, show that the relaxation is complete within several picoseconds.[51,52]

In contrast to the alkali metals, transition metals form structures with distinct energy bands. In particular, the d electron energy bands are distinct in energy from those of the s and p electrons. In addition, the partially filled d orbitals ensure that strong, directional bonding will characterize transition metal chemistry. It is unlikely, therefore, that a delocalized model like the jellium model will adequately describe transition metal clusters. However, a molecular orbital description of any transition metal cluster beyond the level of the triatomic is exceedingly difficult.[49] This is a consequence of the large numbers of electronic states expected. Only for the coinage metals, with $d^{10}s^1$ configurations, are extensive molecular orbital calculations available. These metals share many common characteristics with the alkali metals. For the early transition metals, the situation is much more complex and little is known in detail. The electronic structure of small niobium clusters, Nb_2 to Nb_{10}, has been calculated within the local spin density approximation, but only for geometries frozen in C_{3v} symmetry with bond lengths fixed at either that of the dimer or that of the bulk.[53] The electronic properties of V_6 have been calculated within the linear combination of atomic orbitals (LCAO)-$X\alpha$ scheme. An electronic density of states for the cluster was obtained which was remarkably similar to that for the bulk metal.[54] As in the metal, the consequence of the involvement of d electrons is that there are many low-lying electronic states.

In principle, the electronic density of states for small neutral clusters can be derived from the photoelectron spectrum observed following photodetachment of cluster anions. In practice, some care is required in extracting density of states data from the spectra, but the general conclusion is

that small clusters of transition metals with open d shells have large numbers of low-lying electronic states when the d orbitals are localized on the atoms.[55,56] This observation is in agreement with *ab initio* calculations of Walch and Bauschlicher.[57]

Surface plasmon resonances have been observed for niobium, tantalum, and tungsten metal surfaces at energies in the range of 9 eV following measurements of optical constants.[58-60] However, as noted above, these resonances are expected to be shifted to the red as the cluster size decreases as a consequence of the increased polarizability of the clusters.

Given that transition metal clusters are characterized by many low-lying electronic states and that the optical excitation may be characterized by a collective "surface plasmon" resonance, we propose that the initial excitation is strongly coupled by vibronic interactions. This proposal has been made previously by Smalley *et al.* who suggested that small transition metal clusters typified the "vibronic soup" limit in which coupling between electronic states gives rise to eigenstates which "will tend to be fairly global mixtures of the vibrational and electronic motions available at a given total energy."[22] If this is so and given that small clusters of niobium have been measured to be very strongly bound,[24] our model for the dynamics responsible for the delayed ionization that we have observed is intuitively reasonable.

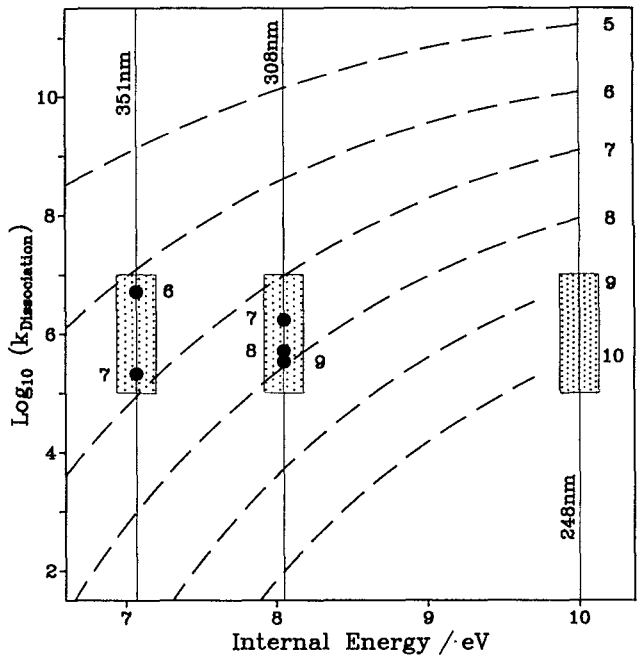

FIG. 13. Results of RRKM modeling of the atom loss from niobium clusters, Nb_n, multiphoton excited to 7.5, 8, and 10 eV at 351, 308, and 248 nm. The dashed lines show dissociation rates calculated via Eq. (A3) for values of n from 5 to 10. The points are data measured in this study for $n = 6$ and 7 at 351 nm and $n = 7$, 8, and 9 at 308 nm. The boxed region shows the accessible measurement space in these experiments. The measurement space at 248 nm is limited to clusters below Nb_9 by direct, single photon ionization.

2. Dissociation and ionization

Before discussing the results of using simple statistical theory to model our data, we point out that it is in qualitative accord with the majority of our results. In particular, it can account for the cluster size and wavelength dependence of the decay times presented in Figs. 6 and 8. This can be understood at a simplistic level by defining the effective temperature, T^*, of a cluster following two-photon excitation:

$$kT^* = (2h\nu_L + E_{th})/(3n - 6), \qquad (10)$$

where E_{th} is the vibrational energy of the cluster prior to photoexcitation. This equation also explains the apparent seven atom effect. Carbon is strongly bound to niobium,[61] yet this binding is unlikely to substantially affect the niobium–niobium binding energy. We have determined that it does not substantially affect the ionization potential.[62] The effect on T^* of the change in vibrational frequency on substitution of niobium by carbon will be small, as at 8 eV the vibrational partition functions will be in their high temperature limits. This is because all vibrational frequencies are low in niobium cluster molecules. Therefore, Eq. (10) should apply, and the most strongly determining factor of the decay rate, the effective temperature, T^*, will be inversely proportional to the number of atoms and will have only a small dependence on their nature. Hence, the rates decrease as a function of cluster size and are more or less equivalent for clusters of the same nuclearity provided that dissociation energies are not strongly affected.

Although the effective temperature of a niobium cluster following two-photon excitation is not strongly dependent upon the nature of the substituent atoms, the subsequent chemistry is. The bond dissociation energy for the niobium dimer is 5.2 eV.[24] That for niobium carbide is approximately the same, 5.9 eV;[61] whereas, the bond dissociation energy for niobium oxide is 8.1 eV.[63] We submit that the very strong bond in niobium oxide makes this molecule a good leaving group. The implication is that partially oxidized niobium clusters preferentially eliminate NbO rather than an electron or a niobium atom in consequence of favorable energetics for the elimination of the diatomic oxide. This, we believe, is why niobium oxide clusters do not show an ionization signal at 308 nm in contrast to niobium and niobium carbide clusters.

Calculations of the dissociation rate for Nb_5 to Nb_{12} following two-photon excitation at 351, 308, and 248 nm were carried out using the generalized cluster Rice–Ramsberger–Kassel–Marcus (RRKM) calculation outlined in the Appendix. The results are shown in Fig. 13. Given the sensitivity of these calculations to a host of unknown molecular parameters (Appendix, Table III), it would be unreasonable to claim an exact fit to experiment or to adjust simply one parameter to fit the model to our experimental results. Rather, we note that our experiment can measure rates in the range 1×10^7 to $1\times10^5\ s^{-1}$ and that our model predicts rates within this window for those situations which give an observable rate in the experiment. These situations are Nb_6 and Nb_7 at 351 nm and Nb_7, Nb_8, and Nb_9 at 308 nm. Therefore, we claim that the model is globally consistent with the observations. Only for Nb_9 at 308 nm is there significant disagreement and there are several potential explanations for this. It is known that Nb_9 exists in at least two isomeric forms in laser-produced cluster beams of the kind

TABLE I. Estimates of ionization and dissociation rates for niobium clusters from RRKM theory.

n	λ/nm	T/K[a]	$k_{diss}/(s^{-1})$[b]	$k'_{diss}/(s^{-1})$[c]	$k'_{ion}/(s^{-1})$[d]	$k_{obs}/(s^{-1})$[e]
5	308	50	1.4×10^{10}	2.7×10^{9}	1.8×10^{8}	$>10^{7}$
6	308	50	3.8×10^{8}	7.2×10^{7}	1.0×10^{7}	$>10^{7}$
7	308	50	9.6×10^{6}	1.7×10^{6}	5.8×10^{5}	1.5×10^{6}
7	308	300	2.9×10^{7}	5.8×10^{6}	1.5×10^{6}	...
7	308	500	6.2×10^{7}	1.4×10^{7}	2.9×10^{6}	...
8	308	50	2.2×10^{5}	3.9×10^{4}	1.0×10^{4}	3.3×10^{5}
9	308	50	4.0×10^{3}	6.8×10^{2}	2.5×10^{4}	2.5×10^{5}
10	308	50	9.1×10^{1}	1.5×10^{1}	3.4×10^{1}	$<10^{5}$
6	351	50	1.0×10^{7}	1.2×10^{6}	3.4×10^{5}	5×10^{6}
7	351	50	7.6×10^{4}	8.3×10^{3}	9.7×10^{3}	2×10^{5}
6	248	50	1.5×10^{10}	4.6×10^{9}	3.5×10^{8}	$>10^{7}$
7	248	50	1.2×10^{9}	3.6×10^{8}	4.2×10^{7}	$>10^{7}$

[a] T_{beam}, see text.
[b] Rate constant calculated using Eq. (A3).
[c] Rate constant calculated using Eq. (A4).
[d] Rate constant calculated using Eq. (A5).
[e] Observed rate constant for decay of Nb_n peak, $(1/\tau_{obs})$. Rates of 10^7–10^5 s^{-1} may be measured in our experiment.

produced in this study.[12-16] It is likely that one isomer would have a lower bond dissociation energy than that estimated via Eq. (A1). That isomer would then have a faster dissociation rate than we have estimated. In addition, the observed decay times are determined by contributions from both ionization and dissociation and it is possible that for Nb_9, the ionization rate is more important (see Table I). In this context we note that the ionization potential of the reactive (to hydrogen chemisorption) form of Nb_9, 4.92 eV, is low in comparison to Nb_8, 5.53 eV, and Nb_{10}, 5.48 eV.

The question of the stability and distinguishability of isomeric forms of clusters of strongly bound atoms is interesting in its own right. For materials, these molecular concepts correlate with phase transitions, particularly the solid–liquid melting transition. The melting point of bulk niobium is very high, 2750 K, and it is possible, *vide infra*, that clusters larger than Nb_7 with 8 eV internal energy maintain distinct isomeric forms.

For tungsten and tantalum, the calculated dissociation rates are far too small to be consistent with the observed decay times. This is a consequence of the extremely large heats of vaporization of these elements.[64] This effectively shuts off the dissociation channel. Rates of 3.4×10^3 and 8.9×10^{-1} s^{-1} are calculated for Ta_7^+ and W_7^+, respectively. Consequently, for these elements it is essential to include the ionization channel in the statistical calculations. This was done for all three elements using the approach outlined in the Appendix. The results for niobium are listed in Table I. For Ta_7 and W_7 at 308 nm, the calculated ionization rates are 2.4×10^6 and 3.0×10^5 s^{-1}, respectively. These are in good agreement with the observed rates (2.5×10^6 and 6.5×10^5 s^{-1}). We note in passing that the observed decay rates for Nb_7, Ta_7, and W_7 are ordered as the work functions of the materials.[40]

As with the comparison to the dissociation data presented in Fig. 13, we do not have a complete set of input parameters with which to confidently assert that our analysis unequivocally supports our model; rather, we note that it is consistent with our observations. Thus, the results for the niobium cluster dissociation rates presented in Fig. 13 are somewhat greater than our experimental values; adding the electronic states of the cluster increases the accessible volume of phase space and slower decay times result (see Table I). In addition, and more importantly, the energetics are substantially different for the dissociation and ionization channels and for Ta_7, W_7, and possibly Nb_9, this is the determining factor.

C. Ladder models for multiphoton dynamics

We commented above that our results are in disagreement with those of Cole and Liu who interpreted their data in terms of the dissociation of ions within the acceleration field of the mass spectrometer.[26] The atom binding energies and ionization potentials of small niobium clusters and the dissociation energies of niobium cluster ions are all in the range of 5 eV.[24] As a 308 nm photon provides only 4 eV, the dissociation of a niobium cluster ion must be preceded by the absorption of at least three 308 nm photons. We may modify our mechanism to account for this possibility by the inclusion of Eqs. (11) to (13),

$$M_n^+ + mh\nu_L \rightarrow M_n^{+*}, \tag{11}$$

$$M_n^{+*} \rightarrow M_n^{+\dagger}, \tag{12}$$

$$M_n^{+\dagger} \rightarrow M_{n-1}^+ + M. \tag{13}$$

These equations applied repetitively in combination with Eqs. (2) to (7) define a ladder model applicable to the response of refractory clusters to multiphoton excitation at high laser intensities where direct multiphoton ionization is the more probable initiation step. This model has much in common with previous models proposed of high intensity behavior, particularly the ladder model of Smalley and coworkers[22] and the thermionic emission model of Riley and co-workers.[65] In all of these models, photon absorption is proposed to proceed indiscriminately until the rate of dissociation or ionization is faster than the rate of photon absorp-

tion. Prompt ionization or dissociation then results to be followed by further indiscriminate absorption of the products to reach dissociating or ionizing states. The overall result is a distribution of ionic fragments which does not represent the original cluster distribution. It is quite conceivable that some of the ionic fragments retain enough energy to dissociate after the laser pulse terminates. Therefore, under these conditions, metastable dissociation of ionic fragments in the acceleration or field-free regions of the mass spectrometer would not be an unlikely process.

D. An analogy with materials properties

In this section, we estimate the ionization and dissociation rates for small niobium clusters and for Ta_7 and W_7 by assuming that the clusters are simply small pieces of the bulk material. Under this assumption, these clusters, when heated to 8 eV by laser photons, behave as small electron emission filaments or *nanofilaments*.

Interestingly, thermally activated ionization in competition with dissociation has also been proposed to account for the multiphoton ionization mass spectra of metal cluster oxides.[63] In that work, large clusters of vanadium, chromium, nickel, and iron oxides were formed and multiphoton excited using excimer laser pulses with fluences in the range 1–10 J cm^{-2}. It was suggested that ionization competed with dissociation and photon absorption. The rate of dissociation was modeled using an RRK formalism and the rate of ionization was modeled by assuming that the cluster was a small fragment of the bulk and applying the Richardson–Dushman relationship for the rate of thermionic emission.[40,66] We have applied an analysis which is similar in spirit, but different in detail and this is outlined below.

The Richardson–Dushman relationship for the thermionic emission current density from macroscopic sized samples of an elemental solid, **J** (electrons nm^{-2} s^{-1}), is[40]

$$\mathbf{J} = AT^2 \exp(-\mathrm{WF}/kT), \tag{14}$$

where A, electrons nm^{-2} s^{-1} K^{-2}, is the Richardson constant (values for various elements are listed in Refs. 40 and 66), and WF is the work function of the material.

Similarly, the rate of evaporation of atoms from an elemental solid, **W** (atoms nm^{-2} s^{-1}), is governed by free energy relationships,[64,66]

$$\mathbf{W} = BT^{-1/2} \exp(-\Delta H^0_{\mathrm{vap}}/kT), \tag{15}$$

where $\Delta H^0_{\mathrm{vap}}$ is the heat of vaporization and values of the empirical constant, B, for various elements are listed in Ref. 66. In principle, one can use **W** and **J** multiplied by the surface area of the cluster (see Appendix) to calculate an emission rate. The problem reduces to determining the temperature, T^*, of the cluster following two-photon absorption. This could be estimated by assuming that the specific heat of the cluster is determined solely by its vibrational modes, i.e., using Eq. (10), but this would ignore both phase changes and the small contribution of the electron gas to the specific heat of a metal. To pursue the analogy with bulk materials, we have estimated T^* by distributing the internal energy of the cluster, $E_{th} + 2h\nu_L$, over n atoms of a material whose heat capacity is precisely equivalent to that of the bulk. Standard thermodynamic tables of the heating curve for the element in question were then used to look up both T^* and the phase of the cluster following two-photon excitation.[64] A crude estimate for $E_{th} \approx (3n-6)kT_{\mathrm{beam}}$ was made assuming that the vibrational temperature, T_{beam}, of the clusters prior to photoexcitation was 50 K.

The results of this analysis are reported in Table II. This table also lists the values of the ionization and dissociation

TABLE II. Rate constants for ionization and dissociation of nanofilaments of refractory transition elements at 308 nm.

			Rate constant/s^{-1}				
			Dissociation		Ionization		Observed
n	T^*/K[a]	Phase[b]	k_D[c]	k'_D[d]	k_I[e]	k'_I[f]	k_{obs}[g]
Niobium							
5	4300	L	2.5×10^5	6.2×10^6	6.0×10^8	2.7×10^7	$>10^7$
6	3500	L	2.2×10^3	9.1×10^4	3.2×10^7	8.8×10^5	$>10^7$
7	3000	L	3.2×10^1	1.9×10^3	2.4×10^6	4.1×10^4	1.5×10^6
8	2750	S–L	2.1×10^0	1.6×10^2	4.9×10^5	2.7×10^3	3.3×10^5
9	2750	S–L	2.3×10^0	1.4×10^2	5.2×10^5	1.2×10^4	2.5×10^5
Tantalum							
7	3250	S–L	1.3×10^1	3.8×10^2	2.1×10^7	7.1×10^5	2.5×10^6
Tungsten							
7	3650	S	4.6×10^1	9.5×10^2	3.1×10^7	2.4×10^6	6.5×10^5

[a] The effective temperature of an n atom cluster following two-photon excitation at 308 nm, interpolated from data in Ref. 64.
[b] The phase of the two-photon excited cluster at T^*, from Ref. 64 (S:solid, L:liquid, S–L:phase transition region).
[c] The dissociation rate calculated using Eq. (15).
[d] The dissociation rate calculated using Eq. (16).
[e] The ionization rate calculated using Eq. (14).
[f] The ionization rate calculated using Eq. (14) and size-specific ionization potentials (see text).
[g] The observed decay rate.

rates calculated using Eqs. (14) and (15). Accompanying these values are those calculated by explicitly accounting for the size dependence of energetics. For the ionization rate, the Richardson–Dushman relationship was modified by substituting the work function by the size-specific ionization potential (see Appendix). The evaporation rate was adjusted for size-dependent effects via the Kelvin equation which expresses the increase in vapor pressure as a consequence of surface curvature.[67] When combined with Eq. 15, Eq. (16) results

$$W = BT^{-1/2} \exp[-(\Delta H^{0}_{vap} - 2/3n^{-1/3}4\pi r^{2}\gamma)/kT], \quad (16)$$

where γ and r are the surface energy and effective radius of an atom (Wigner Seitz parameter) in the bulk material (see Appendix).

It is remarkable how well these approaches do in predicting the cluster size-dependent and wavelength-dependent trends in the observed decay times. The implication is that small clusters of the refractory transition elements, when excited to 8 eV at least, are remarkably similar to bulk materials.

V. CONCLUSIONS

We have presented evidence for a delayed ionization process following two-photon excitation of small niobium, tantalum, and tungsten clusters at 308 and 351 nm. This evidence includes the cluster nuclearity and ionization laser wavelength dependence of the decay rate and the observation of delayed photoelectrons. The changes in the mass spectrum and photoelectron signals as the ionization conditions are varied from direct one photon to delayed, two-photon ionization conditions, simply by changing the laser wavelength, are also compelling.

The decay times have been calculated within the framework of a generalized statistical treatment of cluster dissociation and ionization rates. These rates are sensitive to a host of unknown molecular parameters, but general agreement with experiment is obtained. As more cluster size-dependent molecular parameters become available these rate estimates may be revised. A particular result of these estimates is that the dissociation rates for tungsten and tantalum clusters are small in comparison to the ionization rates. For these elements, the observed rates may correspond to the delayed ionization rates. It is of importance to measure the size-dependent ionization potential for these species.

Clusters in which a transition metal atom is substituted by a carbon atom show similar effects, whereas oxidized clusters do not show a two-photon ionization signal. One explanation for this effect is that the diatomic metal oxide is an excellent leaving group in consequence of its extremely strong chemical bond and therefore, in the case of partially oxidized clusters, dissociation dominates ionization.

The model advanced to explain our observations implied that the observed decay rates will be weakly dependent upon a cluster's internal energy prior to photoexcitation. Experiments are under way to test this implication. Few measures of the internal energy or temperature of a cluster are available even though this is an essential parameter for the interpretation of chemical, dynamical, and spectroscopic data. In this regard, it should be noted that a statistically determined rate process may provide an excellent means to measure this parameter.

The strong chemical bonds and rapid intramolecular energy relaxation processes for small clusters of niobium, tantalum, and tungsten implicit in this work and elsewhere[24] may have important consequences. Firstly, it is possible to heat such clusters with single laser photons without dissociating them. Precise control of the internal temperature of a cluster may be obtained using this approach. Coupled with the ability to adsorb and detect molecules at the surface of metal clusters, we may be able to develop a molecular equivalent of temperature programmed desorption which will enable the determination of size-dependent chemisorption bond strengths. Secondly, the size-specific spectrum of the electronic excitation may be measured via correctly designed, two-color, laser excitation experiments. These measurements will address the question of the nature of the initial electronic excitation. In particular, is a surface plasmon collective excitation an appropriate concept? Finally, the rate of relaxation of the electronic excitation may be measured via autocorrelation studies of direct two-photon ionization using ultrashort laser pulses.

Clearly, well characterized metal clusters may provide models of finite size for many materials properties, both static and dynamic. Here we have reported the first observation of time-resolved thermionic emission. It is hoped that these studies will stimulate further exploration of these interesting molecular systems.

APPENDIX

We have modeled the rate of dissociation and ionization of $M_n^{\dagger *}$, see Eqs. (6) and (7), within the framework of the RRKM theory of unimolecular reactions.[68] In this section, we outline our approach which closely follows that developed by Jarrold and Bower to calculate the unimolecular dissociation rate for small metal clusters.[69] In addition, we describe a modification to this approach in order to incorporate the electronic degree of freedom in a consistent if simplistic fashion and we list values of the required input parameters to apply these calculations to niobium, tantalum, and tungsten clusters.

It is worth noting that no geometrical structure has been experimentally determined for any of the clusters considered in this study. As well, few of the required energetic parameters have been defined by experiment. The approach developed by Jarrold and Bower circumvents these difficulties by defining a consistent statistical treatment of cluster rate processes using input derived from materials properties.[69] These properties then define the vibrational frequencies of the cluster and the threshold energy for dissociation.

We have assumed that the reaction channel is the elimination of a single metal atom. This is consistent with experimental observations for small niobium clusters.[24] We used the same procedure to locate the transition state as did Jarrold and Bower[69] and assumed that the addition of a niobium atom to a niobium cluster proceeds without an activation barrier, equating the threshold energy with the atom

binding energy for a particular cluster.

Dissociation energies, D_n^0, have been measured for Nb_2 to Nb_6 and for these clusters we use the measured values.[24] Following Jarrold and Bower,[69] we use Eq. (A1), in which the surface free energy parameter, γ, interpolates between the measured values and the heat of sublimation of the bulk material, ΔH_{vap}^0, to obtain purely empirical estimates of the atom binding energies, both for niobium clusters larger than the hexamer and for all tantalum and tungsten clusters.

$$D_n^0 = D^0(\text{Nb}_{n-1} - \text{Nb}) = \Delta H_{\text{vap}}^0 - 4\pi r^2\gamma \times [n^{2/3} - (n-1)^{2/3}]. \quad \text{(A1)}$$

This equation is derived from the assumption that the cohesive energy of a cluster, $E_c(n)$, can be written in the form

$$E_c(n) = n\Delta H_{\text{vap}}^0 - A_n\gamma, \quad \text{(A2)}$$

where A_n is the surface area of the cluster, $A_n = 4\pi R_n^2$. $R_n = rn^{1/3}$, is the radius of the cluster calculated assuming that it is spherical with a density equivalent to that of the bulk material. The effective radius of an atom in the bulk is given by r.

In connection with the analogy to bulk materials properties outlined in Sec. V [Eq. (16)], we note that the factor $[n^{2/3} - (n-1)^{2/3}]$ rapidly approaches $2/3n^{-1/3}$ as n increases (to within 90% at $n = 2$ and 98% at $n = 9$). Equation (A1) is therefore consistent with the Kelvin equation.[67]

The vibrational frequencies of the clusters were estimated empirically using the scheme suggested by Jarrold and Bower.[69] The vibrational frequencies are derived from the Debye temperature, Θ_D, of the bulk material assuming a distribution of frequencies similar to that used in the Debye theory of the specific heat of metals.[40] The model is parameterized to smoothly extrapolate from the dimer frequency, ν_D, which has been calculated for niobium,[70] to the Debye distribution. The model was applied by Jarrold and Bower to the dissociation of aluminum cluster ions with some success.[69] It has also been applied to the collision induced dissociation of niobium cluster ions by Armentrout and coworkers.[24] They used a Debye frequency for niobium of 1200 cm^{-1} which implies a Debye temperature of 1700 K, whereas low temperature specific heat data imply a Debye temperature of 250 K.[71] We have used the latter value.

From RRKM theory, the rate of dissociation of $M_n^{\dagger *}$ is given by

$$k_{\text{dissociation}} = n \times N(2h\nu_L + E_{th} - D_n^0)/ h \times \rho(2h\nu_L + E_{th}), \quad \text{(A3)}$$

where $\rho(E)$ represents the density of states in the cluster at an internal energy E and $N(E)$ represents the total number of states of the cluster transition state up to an energy E.[68] Both $\rho(E)$ and $N(E)$ were evaluated by direct counting using the Beyer–Swinehart algorithm.[72] Following Jarrold and Bower, we equate the reaction path degeneracy with the number of surface atoms;[69] in a small cluster this is equal to n, the total number of atoms. For larger clusters, a value of $n^{2/3}$ may be more appropriate.[69] We have included a contribution to the total internal energy of a cluster from the thermal population of its vibrational modes prior to the photoexcitation through the factor E_{th} [$\approx (3n-6)kT_{\text{beam}}$] in order to be able to assess the effects of the initial temperature of the clusters upon the observed rate. This internal energy could be calculated more exactly via vibrational partition functions, implicit from the vibrational density of states, but, in view of the level of approximation of the approach, this degree of detail is unwarranted at the present time. The initial vibrational temperature of the clusters in our experiments, T_{beam}, is not well defined. If the expansion is well developed and vibrational cooling were efficient, then T_{beam} would be low. If, on the other hand, the temperature of the clusters were determined by the heat of condensation, T_{beam} would be high. The uncertainty in T_{beam} offers a mechanism by which to explore source-dependent contributions to the observed rates.

We have modeled the ionization rate under a statistical approximation with the following highly simplified model in which we assume that the vibrational states of a cluster may

TABLE III. Input parameters for generalized statistical calculations of ionization and dissociation rates for refractory metal clusters.

Parameter[a]	Units	Niobium	Tantalum	Tungsten	Sensitivity[b]
ΔH_{vap}^0	eV	7.62	8.13	8.85	↓
γ	eV nm^{-2}	1.2×10^{-3}	1.4×10^{-3}	1.4×10^{-3}	↑
Θ_D	K	250	230[c]	370[d]	↑
ν_D	cm^{-1}	450	350[e]	350[e]	↑
WF	eV	4.3	4.1	4.55	↓
r	nm	0.147	0.147	0.141	↓
T_{beam}	K	50	50	50	↑

[a] See text. Surface energies, densities, and work functions were selected from values listed in *Handbook of Chemistry and Physics*, edited by D. R. Lide (CRC, Boca Raton, 1990).

[b] This column indicates the sensitivity of the calculated dissociation rate constant to variation in the indicated parameter. An entry marked ↑ indicates that the calculated rate increases when the value of the parameter is increased; for entries marked ↓, the opposite is true. The entries under WF and r show the sensitivity of the ionization rate to variation in these parameters.

[c] K. F. Sterret and W. E. Wallace, J. Am. Chem. Soc. **80**, 3176 (1958).

[d] W. Desorbo, J. Phys. Chem. **62**, 965 (1958).

[e] Estimated value.

freely exchange energy with the electronic degrees of freedom.

The problem is to characterize the number of electronic states as a function of energy. We have taken the simplest possible approach to this problem by assuming a single electron model. We assume that the electronic degree of freedom has energy levels and degeneracies given by those of an electron confined in a spherical box whose radius is given by the radius of the cluster, R_n.[73] We assume that the transition state for ionization is one in which this electronic degree of freedom is removed and that the threshold energy for the process is given by the ionization potential. Following Eq. (A3), the rates of ionization and dissociation are given by

$$k'_{\text{dissociation}} = n \times N'_D(2h\nu_L + E_{th} - D_n^0)/ h \times \rho'(2h\nu_L + E_{th}), \quad \text{(A4)}$$

$$k'_{\text{ionization}} = N'_I(2h\nu_L + E_{th} - IP_n)/ h \times \rho'(2h\nu_L + E_{th}), \quad \text{(A5)}$$

where $N'_D(E)$ and $N'_I(E)$ refer to the total number of *vibronic* states below an energy E in the cluster dissociation and ionization transition states, respectively, and $\rho'(E)$ is the density of *vibronic* states in the cluster at an energy E. These quantities were calculated by the direct count procedure, as modified by Stein and Rabinovitch,[74] to take account of the fact that the energy levels in the electronic degree of freedom were not equally spaced.

The treatment of the electronic degree of freedom outlined above is highly arbitrary. Other formulations of the density of electronic states as a function of internal energy, for instance a Rydberg expression, may be more appropriate. These approaches could also be incorporated within the framework outlined above. It is hoped that reliable estimates of the density of electronic states as a function of internal energy will become available from electronic structure calculations. However, we believe that this simplified picture captures the essential aspects of the problem.

As the ionization potential, IP_n, of all niobium clusters up to Nb_{76} have been measured, we are able to use measured and not extrapolated values for this parameter.[16] Where it is known that a cluster has two isomers with different ionization potentials, we have used the lower of the reported values. In principle, there should be an isomer specific ionization rate as a consequence. This may be reflected in an ionization decay which is the sum of two exponential terms. Biexponential decays are observed for Nb_8, Nb_9, and Nb_{10}, although other factors may account for this.

For tantalum and tungsten, no size-specific ionization potentials are available. The ionization potentials of small metal clusters as a function of size have been parameterized within the conducting spherical droplet model,[5]

$$IP_n = \text{WF} + 3e^2/8R_n. \quad \text{(A6)}$$

This model accounts for size-dependent, electrostatic image charge effects and works remarkably well for alkali metal clusters. It fails, however, for clusters of nickel,[75] iron,[76] cobalt,[76] and niobium,[16] and empirical equations have been developed in which the work function term in Eq. (A6) is adjusted. It has been argued that this is because the bulk work function is not applicable to small transition metal clusters. However, the ionization potentials for Nb_{15} to Nb_{76} are within the range 4.7 ± 0.1 eV, which is close to the work function of the bulk, 4.3 eV. Similar considerations apply to iron, nickel, and cobalt clusters. It could be concluded from this that transition metal clusters in this size range are surprisingly similar to bulk materials. Consequently, we have used Eq. (A7) which adequately fits the known data for niobium, iron, nickel, and cobalt to derive purely empirical estimates for the size-specific ionization potentials of tantalum and tungsten clusters.

$$IP_n = \text{WF} + 0.2/R_n \quad \text{(A7)}$$

in which the energies are in eV and R_n is in nm. Ionization potentials of 5.04 and 5.49 eV were derived for Ta_7 and W_7, respectively.

Table III lists values of the input parameters required to apply the models outlined above to clusters of niobium, tantalum, and tungsten. Also included in Table III is an indication of the sensitivity of the calculated rate to variation in the value of the input parameter.

[1] R. P. Andres, R. S. Averback, W. L. Brown, L. E. Brus, W. A. Goddard III, A. Kaldor, S. G. Louie, M. Moscovits, P. S. Peercy, S. J. Riley, R. W. Siegel, F. Spaepen, and Y. Wang, J. Mater. Res. **4**, 704 (1989).
[2] M. E. Geusic, M. D. Morse, and R. E. Smalley, J. Chem. Phys. **82**, 590 (1985).
[3] M. D. Morse, M. E. Geusic, J. R. Heath, and R. E. Smalley, J. Chem. Phys. **83**, 2293 (1985).
[4] D. M. Cox, K. C. Reichmann, D. J. Trevor, and A. Kaldor, J. Chem. Phys. **88**, 111 (1988).
[5] R. L. Whetten, M. R. Zakin, D. M. Cox, D. J. Trevor, and A. Kaldor, J. Chem. Phys. **85**, 1697 (1986).
[6] R. L. Whetten D. M. Cox, D. J. Trevor, and A. Kaldor, Phys. Rev. Lett. **54**, 1494 (1985).
[7] J. C. Phillips, J. Chem. Phys. **84**, 1951 (1986).
[8] K. C. C. Kharas, Chem. Phys. Lett. **161**, 339 (1989).
[9] M. R. Zakin, D. M. Cox, D. J. Trevor, R. L. Whetten, and A. Kaldor, Chem. Phys. Lett. **133**, 223 (1987).
[10] L. -S. Zheng, P. J. Brucat, C. L. Pettiette, S. Yang, and R. E. Smalley, J. Chem. Phys. **83**, 4273 (1985).
[11] J. L. Elkind, F. D. Weiss, J. M. Alford, R. T. Laaksonen, and R. E. Smalley, J. Chem. Phys. **88**, 5215 (1988).
[12] M. R. Zakin, R. O. Brickman, D. M. Cox, and A. Kaldor, J. Chem. Phys. **88**, 3555 (1988).
[13] Y. Hamrick, S. Taylor, G. W. Lemire, Z. -W. Fu, J. -C. Shui, and M. D. Morse, J. Chem. Phys. **88**, 4095 (1988).
[14] Y. M. Hamrick and M. D. Morse, J. Phys. Chem. **93**, 6494 (1989).
[15] M. B. Knickelbein and S. Yang, J. Chem. Phys. **93**, 1476 (1990).
[16] M. B. Knickelbein and S. Yang, J. Chem. Phys. **93**, 5760 (1990).
[17] R. J. St. Pierre, E. L. Chronister, and M. A. El-Sayed, SPIE **742**, 122 (1987), R. J. St. Pierre and M. A. El-Sayed, J. Phys. Chem. **91**, 763 (1987).
[18] M. R. Zakin, D. M. Cox, and A. Kaldor, J. Phys. Chem. **91**, 5244 (1987).
[19] M. R. Zakin, R. O. Brickman, D. M. Cox, and A. Kaldor, J. Chem. Phys. **88**, 5943 (1988).
[20] R. J. St. Pierre, E. L. Chronister, and M. A. El-Sayed, J. Phys. Chem. **91**, 5228 (1987).
[21] L. Song and M. A. El-Sayed, Chem. Phys. Lett. **152**, 281 (1988).
[22] P. J. Brucat, L. -S. Zheng, C. L. Pettiette, S. Yang, and R. E. Smalley, J. Chem. Phys. **84**, 3078 (1986).
[23] S. K. Loh, L. Lian, D. Hales, and P. B. Armentrout, J. Chem. Phys. **89**, 3378 (1988).
[24] S. K. Loh, L. Lian, and P. B. Armentrout, J. Am. Chem. Soc. **111**, 3167 (1989).
[25] S. K. Loh, L. Lian, and P. B. Armentrout, J. Chem. Phys. **91**, 6148 (1989).
[26] S. K. Cole and K. Liu, J. Chem. Phys. **89**, 780 (1988).
[27] S. K. Cole, K. Liu, and S. K. Riley, NATO ASI Series B: Physics Vol. 158,

Physics and Chemistry of Small Clusters, edited by P. Jena, B. K. Rao, and S. N. Khanna (Plenum, New York, 1987), pp. 347–352.
[28] M. E. Geusic, M. D. Morse, S. C. O'Brien, and R. E. Smalley, Rev. Sci Instrum. **56**, 2123 (1985); M. D. Morse, M. E. Geusic, J. R. Heath, and R. E. Smalley, J. Chem. Phys. **83**, 2293 (1985).
[29] D. A. Dahl, J. E. Delmore, and A. D. Appelhans, Rev. Sci. Instrum. **61**, 607 (1990).
[30] W. C. Wiley and I. H. McLaren, Rev. Sci. Instrum. **26**, 1150 (1955).
[31] C. L. Callender, D. M. Rayner, and P. A. Hackett, Appl. Phys. B **47**, 7 (1988).
[32] R. G. Cooks, J. H. Beynon, R. M. Caprioli, and G. R. Lester, *Metastable Ions* (Elsevier, Amsterdam, 1973).
[33] A. Amrein, R. Simpson, and P. A. Hackett, J. Chem. Phys. **94**, 4663 (1991).
[34] R. S. Berry, J. Chem. Phys. **45**, 1228 (1966); R. S. Berry and S. E. Nielson, Phys. Rev. A **1**, 383 (1970).
[35] F. X. Campos, Y. Jing, and E. R. Grant, J. Chem. Phys. **93**, 2308 (1990).
[36] R. F. Foster, W. Tumas, and J. I. Brauman, J. Chem. Phys. **79**, 4644 (1983).
[37] R. N. Compton, L. G. Christophorou, G. S. Hurst, and P. W. Reinhart, J. Chem. Phys. **45**, 4634 (1966).
[38] L. G. Christophorou, Adv. Electron. Electron Phys. **46**, 55 (1978).
[39] J. J. Ewing, R. Milstein, and R. S. Berry, J. Chem. Phys. **54**, 1752 (1971).
[40] J. S. Blakemore, *Solid State Physics*, 2nd ed. (Cambridge University, Cambridge, 1985), pp. 188–192.
[41] E. P. Wigner and F. Seitz, Phys. Rev. **43**, 804 (1933).
[42] J. C. Phillips, Chem. Rev. **86**, 619 (1986).
[43] C. Brechignac, Ph. Chazuzac, F. Carlier, M. de Frutos, and J. Leygnier, J. Chem. Soc. Faraday Trans. **86**, 2525 (1990).
[44] T. P. Martin, T. Bergmann, and N. Malinowski, J. Chem. Soc. Faraday Trans. **86**, 2489 (1990), and references cited therein.
[45] W. A. de Herr, K. Selby, V. Kresin, J. Masui, M. Volmer, A. Chatelain, and W. Knight, Phys. Rev. Lett. **52**, 2141 (1984).
[46] V. Kresin, Phys. Rev. B, **39**, 3042 (1989).
[47] C. R. C. Wang, S. Pollack, D. Cameron, and M. Kappes, J. Chem. Phys. **93**, 3787 (1990).
[48] V. Bonacic-Koutecky, P. Fantucci, and J. Koutecky, J. Chem. Phys. **93**, 3802 (1990); J. Koutecky and P. Fantucci, Chem. Rev. **86**, 539 (1986).
[49] D. M. P. Mingos, T. Slee, and L. Zhenyang, Chem. Rev. **90**, 383 (1990).
[50] K. Selby, M. Volmer, J. Masui, V. Kresin, W. A. de Heer, and W. D. Knight, Phys. Rev. B **40**, 5417 (1989).
[51] M. van Exter and A. Lagendijk, Phys. Rev. Lett. **60**, 49 (1988).
[52] H. E. Elsayed-Ali, T. B. Norris, M. A. Pessot, and G. A. Mourou, Phys. Rev. Lett. **58**, 1212 (1987).
[53] T. Wahnstrom, A. Rosen, and T. T. Rantala, NATO ASI Series B: Physics Vol. 158, *Physics and Chemistry of Small Clusters*, edited by P. Jena, B. K. Rao, and S. N. Khanna (Plenum, New York, 1987), pp. 511–516.
[54] G. Seifert and H. Eschrig, Phys. Stat. Sol. B **127**, 573 (1985).
[55] J. Ho, K. M. Ervin, and W. C. Lineberger, J. Chem. Phys. **93**, 6987 (1990).
[56] G. Gantefor, M. Gaussa, K-H. Meiwes-Broer, and H. O. Lutz, J. Chem. Soc. Faraday Trans. **86**, 2483 (1990).
[57] S. P. Walch and C. W. Bauschlicher, in *Quantum Chemistry: The Challenge of Transition Metals and Coordination Chemistry*, edited by A. Veillard (Reidel, Dordrecht, 1986), p. 119.
[58] J. H. Weaver, D. W. Lynch, and C. G. Olson, Phys. Rev. B **7**, 4311 (1973).
[69] J. H. Weaver, D. W. Lynch, and C. G. Olson, Phys. Rev. B **10**, 501 (1974).
[60] J. H. Weaver, C. G. Olson, and D. W. Lynch, Phys. Rev. B **12**, 1293 (1975).
[61] J. B. Pedley and E. M. Marshall, J. Phys. Chem. Ref. Data **12**, 967 (1984).
[62] A. Amrein, R. Simpson, and P. A. Hackett (unpublished).
[63] S. K. Gupta and K. A. Gingerich, J. Chem. Phys. **74**, 3584 (1981).
[64] M. W. Chase, C. A. Davies, J. R. Downey, Jr., D. J. Fripp, R. A. McDonald, and A. N. Syverud, J. Phys. Chem. Ref. Data **14**, 1601 (1985).
[65] C. Nieman, E. K. Parks, S. C. Richtsmeier, K. Liu, L. G. Pobo, and S. J. Riley, High Temp. Sci. **22**, 115 (1986).
[66] S. Dushman and J. M. Lafferty, *Scientific Foundations Vacuum Technique*, 2nd ed. (Wiley, New York, 1962), pp. 691–703.
[67] A. A. Adamson, *Physical Chemistry of Surfaces*, (Wiley, New York, 1990).
[68] W. Forst, *Theory of Unimolecular Reactions* (Academic, New York, 1973).
[69] M. F. Jarrold and J. E. Bower, J. Chem. Phys. **87**, 5728 (1987).
[70] S. P. Walch and C. W. Bauschlicher, Jr., *Comparison of Ab Initio Quantum Chemistry with Experiment*, edited by E. J. Bartlett (Reidel, Dordrecht, 1985).
[71] J. F. DaSilva, E. A. Burgemeister, and Z. Dokoupil, Physica, **41**, 409 (1969).
[72] T. Beyer and D. F. Swinehart, Commun. Assoc. Comput. Machin. **16**, 379 (1973).
[73] O. K. Rice, *Statistical Mechanics, Thermodynamics, and Kinetics* (Freeman, San Francisco, 1967).
[74] S. E. Stein and B. S. Rabinovitch, J. Chem. Phys. **58**, 2438 (1973).
[75] M. B. Knickelbein, S. Yang, and S. J. Riley, J. Chem. Phys. **93**, 94 (1990).
[76] S. Yang and M. B. Knickelbein, J. Chem. Phys. **93**, 1533 (1990).